Molecular theory of a ferromagnetic nematic liquid crystal

Immanuel S. Geier,[1] Stefanie M. Wandrei,[1] Robert A. Skutnik,[1] and Martin Schoen[1,2,3]

[1]*Stranski-Laboratorium für Physikalische und Theoretische Chemie, Fakultät für Mathematik und Naturwissenschaften, Technische Universität Berlin, Straße des 17. Juni 115, 10623 Berlin, Germany*

[2]*Department of Chemical Engineering, Imperial College London, South Kensington Campus, London SW7 2AZ, United Kingdom*

[3]*Department of Chemical and Biomolecular Engineering, Engineering Building I, Box 7905, North Carolina State University, 911 Partners Way, Raleigh, North Carolina 27695, USA*

(Received 24 May 2019; revised manuscript received 24 July 2019; published 13 August 2019)

We employ a version of classical density functional theory to study the phase behavior of a simple model liquid crystal in an external field. The uniaxially symmetric molecules have a spherically symmetric core with superimposed orientation-dependent attractions. The interaction between the cores consists of a hard-sphere repulsion plus an isotropic square-well attraction. The anisotropic part of the interaction potential allows for the formation of a uniaxially symmetric nematic phase. The orientation of the molecules couples to an external polar field. The external field is capable of rotating the nematic director $\widehat{\boldsymbol{n}}$ in the x-z plane. The field is also capable of changing the topology of the phase diagram in that it suppresses the phase coexistence between an isotropic liquid and a nematic phase observed in the absence of the field. We study the transition from an unpolar to a polar nematic phase in terms of the orientation-distribution function (odf), nematic and polar order parameters, and components of $\widehat{\boldsymbol{n}}$. If represented suitably the odf allows us to study orientational changes during the switching process between nonpolar and polar nematic phases. We also give a simple argument that explains why nematic order is lost whereas polar order persists up to the gas-liquid critical point along the coexistence curve. We also discuss the relevance of our theory for future experimental studies.

DOI: 10.1103/PhysRevE.100.022702

I. INTRODUCTION

Because of the technological importance a large body of fundamental scientific work already exists that is devoted to various aspects of the interaction between liquid-crystalline materials and external fields. For instance, Camacho-Lopez *et al.* [1] studied orientationally ordered liquid-crystal elastomers exposed to mechanical strain. This strain is perceived as the external field in their case. In a more recent review Leferink op Reinink *et al.* [2] discuss the impact of various external fields on lyotropic colloidal liquid crystals. Besides the perhaps more conventional electric or magnetic fields these authors also consider the impact of the Earth's gravitational field.

In another system polymers are used to stabilize blue phases that can be formed in chiral liquid crystals [3]. The polymer matrix acts as an "external field" in this example. Blue phases are normally stable over a very narrow temperature range of less than a few K. By adding the polymer, Kikuchi *et al.* [3] were able to widen the range of stability to about 60 K. This achievement is very important because blue phases can be used as electro-optical switches with very short response times of about 10^{-4} s.

In most studies to date external electric fields have been used to manipulate liquid crystals (see also the review article by Garbovskiy and Glushchenko [4] and references therein). For example, Kim *et al.* [5] used an electric field to reversibly switch nematic domains of a liquid crystal. This is important to reduce the power consumption required for high-information-content displays. In another study [6], the electro-optical and thermo-optical properties of liquid crystals have been investigated. The authors studied the effects of applied voltage and temperature on liquid-crystal droplet morphology and its transmission characteristics. In a composite system in which one of the compounds consists of a chiral nematic liquid crystal, Hu *et al.* [7] investigated the electrically controllable selective reflectivity of their hybrid system.

Using magnetic fields van den Pol *et al.* [8] were able to stabilize biaxial nematic and biaxial smectic phases in a colloidal model system consisting of boardlike goethite particles. Ostapenko *et al.* [9] studied the magnetic-field induced isotropic-nematic phase transition in bent-core liquid-crystalline materials. The critical magnetic field to initiate this phase transition increases with temperature. The authors employ Landau–de Gennes (LdG) [10] and Maier-Saupe [11] mean-field models to rationalize their experimental findings.

Particularly fascinating liquid-crystalline systems are those exhibiting unpolar and polar nematic order at the same time. The idea that this could happen is quite old. In fact, Born [12,13] introduced the hypothesis that attractive dipolar interactions would allow for the formation of ordered liquidlike phases. The mechanism through which this happens is one in which the configurational energy in an ordered phase can be lower than that of a corresponding isotropic liquid phase. In his work, Born applied a simple mean-field approximation to describe the isotropic-nematic phase transition. Because his system is composed of dipoles the nematic phase turns out to be also polar (ferroelectric nematic) with the dipoles aligned with the nematic director.

Quite some time later Brochard and de Gennes [14] in a seminal paper considered a suspension of small magnetic particles in a nematic carrier fluid. They developed a continuum theory for this ferromagnetic nematic liquid crystal that has at its core the assumption that the magnetization is always perfectly aligned with the nematic director. This is sometimes referred to as the "rigid anchoring" condition [15]. However, as pointed out in a recent review article by Mertelj and Lisjak (see Ref. [16] and references therein) progress in experimental studies of ferromagnetic nematic liquid crystals has been relatively slow for many years. The main obstacle hampering this progress was the difficulty to sufficiently stabilize ferromagnetic nematic phases. This problem could only be mastered fairly recently [17].

Experimentally, ferromagnetic ordering arises in suspensions of magnetic nanoplatelets in a nematic carrier fluid [17]. If the anchoring of the liquid-crystal molecules is sufficiently strong and parallel to the surface of the platelets, the spontaneous magnetization $\boldsymbol{M}$ will align with the nematic director $\hat{\boldsymbol{n}}$ [18–20]. If now a magnetic field is applied in a direction perpendicular to $\boldsymbol{M}$ it exerts a torque on the nanoplatelets which reorients them. This also reorients $\hat{\boldsymbol{n}}$ through the anchoring of the liquid-crystal molecules at the surface of the platelets. Because of the spatial variation of $\hat{\boldsymbol{n}}$ in the presence of an external magnetic field the optical properties of the nematic host phase will change in a controllable manner [21,22] (see also Figs. 1 and 2 of Ref. [19] and Fig. 1 of Ref. [20]). Besides nanoplatelets, suspensions of rodlike and spherical nanoparticles in a nematic carrier fluid have also been considered [23].

On the theoretical side and after Brochard and de Gennes' theory [14] quite a bit of work has been carried out to understand various aspects of ferromagnetic nematic phases [24–28]. However, these theoretical works are all based upon a macroscopic (continuum) picture.

The goal of the present study is to contribute to our understanding of ferromagnetic nematic liquid crystals at the *molecular* level. We are employing classical density functional theory (DFT) in the version proposed recently by Schoen *et al.* [29] in which the short-range positional order is accounted for realistically. Unlike computer simulations, DFT has the advantage that it is numerically very efficient and avoids the notorious finite-size effects [30] in computer simulations of ordered liquid-crystalline materials.

We are essentially using a model that has been proposed originally by Maier and Saupe [11]; later a more sophisticated version of this model has been suggested by Hess and Su [31]. This model is capable of exhibiting nematic order. In addition, we are allowing the orientations of the mesogens to couple to a polar external field. That way our model liquid crystal is capable of exhibiting properties of a ferromagnetic nematic phase.

The remainder of this paper is organized as follows. In Sec. II our model system is introduced. We develop an approximate free-energy functional in Sec. III. Section IV is devoted to aspects of minimizing the grand-potential density. We introduce key quantities on which this work is based in Sec. V and present our results in Sec. VI. These results are discussed and summarized in Sec. VII.

The paper has three Appendixes. In Appendix A we demonstrate that the orientation dependence of intermolecular interactions in our model is equivalent to the one proposed by Hess and Su [31], Appendix B is devoted to mathematical details in the development of the free-energy functional, and in Appendix C we analyze the alignment tensor $\mathbf{Q}$ for a perfectly ordered ferromagnetic nematic phase.

II. MODEL

A. Intermolecular interactions

We consider a simple model of a thermotropic liquid crystal composed of N molecules (mesogens) interacting with each other in a pairwise additive fashion. The interaction potential is assumed to consist of two parts: one of them describes the interaction between the spherically symmetric cores of a pair of mesogens, the other one accounts for the orientation dependence of the interactions. Thus, we can decompose the total interaction potential according to

$$u(\boldsymbol{r}_{12},\omega_1,\omega_2) = u_{\rm iso}(r_{12}) + u_{\rm aniso}(\boldsymbol{r}_{12},\omega_1,\omega_2), \tag{2.1}$$

for a pair of mesogens where the centers of mass are located at $\boldsymbol{r}_1$ and $\boldsymbol{r}_2$, respectively; $\boldsymbol{r}_{12} = \boldsymbol{r}_1 - \boldsymbol{r}_2$ and $r_{12} = |r_{12}|$. In Eq. (2.1), $\omega_i = (\theta_i, \varphi_i)$ $(i = 1, 2)$ are sets of Euler angles that we introduce to specify the orientations of the uniaxial mesogens; in the usual way, θ_i and φ_i denote the polar and azimuthal angle, respectively.

For the short-range repulsive interactions between the isotropic cores we adopt the potential [29]

$$u_{\rm hs}(r_{12}) = \begin{cases} \infty, & r_{12} \leqslant \sigma \\ 0, & r_{12} > \sigma \end{cases} \tag{2.2}$$

for a pair of hard spheres of diameter σ. To derive an explicit functional form for $u_{\rm aniso}$ we follow Gray and Gubbins [32] who pointed out that *any* function that depends on $\boldsymbol{r}_{12}$, ω_1, and ω_2 as its variables can be expanded in the basis of so-called rotational invariants $\{\Phi_{l_1 l_2 l}\}$ according to

$$u_{\rm aniso}(\boldsymbol{r}_{12},\omega_1,\omega_2) = \sum_{l_1 l_2 l} u_{l_1 l_2 l}(r_{12})\Phi_{l_1 l_2 l}(\omega_1,\omega_2,\omega), \tag{2.3}$$

where ω is a set of Euler angles allowing us to specify the orientation of $\hat{\boldsymbol{r}}_{12} = \boldsymbol{r}_{12}/r_{12}$ in a space-fixed frame of reference, $\{u_{l_1 l_2 l}\}$ are expansion coefficients that depend only on r_{12}, and l' (that is l_1, l_2, or l) is a positive semidefinite integer. Throughout this paper the caret will be used to indicate a unit vector.

Members of the set $\{\Phi_{l_1 l_2 l}\}$ form a complete *orthogonal* basis (see Appendix B of Ref. [29]) in which

$$\Phi_{l_1 l_2 l}(\omega_1,\omega_2,\omega) = \sum_{m_1 m_2 m} C(l_1 l_2 l; m_1 m_2 m) \times \mathcal{Y}_{l_1 m_1}(\omega_1)\mathcal{Y}_{l_2 m_2}(\omega_2)\mathcal{Y}^*_{lm}(\omega). \tag{2.4}$$

In Eq. (2.4), C is a Clebsch-Gordan coefficient, $\mathcal{Y}_{l'm'}$ is a spherical harmonic, and the asterisk denotes the complex conjugate; m' (that is m_1, m_2, or m) is an integer that is linked to l' through the relation $m' \in [-l', l']$ so that for each value of l' the corresponding sum over m' comprises $2l' + 1$ terms. Thus, the expansion in Eq. (2.3) has to be truncated for rather small values of l' to be computationally tractable.

To that end we introduce the assumption that $u_{\rm aniso}$ in Eq. (2.1) (and therefore u) should depend only on r_{12} (but

not on the distance *vector* $\boldsymbol{r}_{12}$). This immediately suggests $l = m = 0$ in Eq. (2.4) and therefore $\mathcal{Y}^*_{lm} = \mathcal{Y}_{00} = 1/\sqrt{4\pi}$.

Nonzero Clebsch-Gordan coefficients are then obtained provided the two selection rules [see Eqs. (A.130) and (A.131) of Ref. [32]], (i) $m = m_1 + m_2$ and (ii) $|l_1 - l_2| \leqslant l \leqslant l_1 + l_2$ (triangle inequality), are satisfied simultaneously. Because $m = 0$ the first of these requires $m_1 = -m_2$ whereas for $l = 0$ the triangle inequality suggests $l_1 = l_2$. Therefore the summation over l_1, l_2, m_1, and m_2 in Eqs. (2.3) and (2.4) collapses to

$$\begin{aligned}&\frac{u_{000}(r_{12})}{(4\pi)^{3/2}} + \frac{1}{\sqrt{4\pi}}\sum_{l>0}^{\infty} u_{ll0}(r_{12}) \sum_{m=-l}^{l} C(ll0; m\underline{m}0) \\ &\quad\times \mathcal{Y}_{lm}(\omega_1)\mathcal{Y}_{l\underline{m}}(\omega_2) \\ &= \frac{u_{000}(r_{12})}{(4\pi)^{3/2}} + \frac{1}{(4\pi)^{3/2}}\sum_{l>0}^{\infty}(-1)^l\sqrt{2l+1} \\ &\quad\times u_{ll0}(r_{12})P_l(x),\end{aligned} \tag{2.5}$$

where $\underline{m} = -m$; we also used Eq. (A.157) of Ref. [32] together with $(-1)^m\mathcal{Y}_{l\underline{m}} = \mathcal{Y}^*_{lm}$ and treated the isotropic contribution u_{000} separately. Last but not least, we invoke the addition theorem for spherical harmonics [see Eq. (A.33)]. In Eq. (2.5),

$$x = \cos\gamma = \hat{\boldsymbol{u}}(\omega_1)\cdot\hat{\boldsymbol{u}}(\omega_2) \equiv \hat{\boldsymbol{u}}_1\cdot\hat{\boldsymbol{u}}_2, \tag{2.6}$$

and members of the set $\{P_l\}$ are Legendre polynomials.

At this stage we introduce three more assumptions. First, we require u_{aniso} to remain invariant if the orientation of one of the two mesogens is inverted. This takes notice of the "head-tail" symmetry (i.e., the equivalence of $\hat{\boldsymbol{u}}_i$ and $-\hat{\boldsymbol{u}}_i$) characteristic of many mesogens [10]. In general, P_{2l+1} contains only odd powers of $\cos\gamma$ and thus would change sign if the orientation of one of the two mesogens is inverted, that is if $\gamma \to \gamma' = \gamma \pm \pi$. Hence, we consider only even l (including the even integer $l = 0$) to maintain the desired invariance of u_{aniso}.

Second, we limit ourselves to the leading ($l = 2$) term in the summation in Eq. (2.5) which permits us to introduce

$$u_{\text{iso}}(r_{12}) = u_{\text{hs}}(r_{12}) + \frac{u_{000}(r_{12})}{(4\pi)^{3/2}}, \tag{2.7a}$$

$$u_{\text{aniso}}(r_{12},\omega_1,\omega_2) = \frac{\sqrt{5}}{(4\pi)^{3/2}}u_{220}(r_{12})P_2(x), \tag{2.7b}$$

where $P_2(x) = \frac{1}{2}(3x^2 - 1)$. Thus, the orientation dependence of the anisotropic interactions in Eq. (2.7b) is the same as that used by Mayer and Saupe [see Eq. (1) of Ref. [11]] and also by Hess and Su [31] for the special case in which only the coupling constant ϵ_1 in their Eq. (9) is nonzero. To demonstrate the equivalence between our Eq. (2.7b) and the corresponding expressions in the paper by Hess and Su [31] is slightly more involved. We summarize the main steps of this demonstration in Appendix A.

The expansion coefficients u_{000} and u_{220} in Eqs. (2.7) are still undetermined. Unfortunately, within the present approach we cannot resort to any first principles to determine the expansion coefficients. Instead, we need to make an ansatz by introducing as our third assumption

$$\frac{u_{000}(r_{12})}{(4\pi)^{3/2}} = u_{\text{sw}}(r_{12}), \tag{2.8a}$$

$$\frac{\sqrt{5}}{(4\pi)^{3/2}}u_{220}(r_{12}) = \varepsilon' u_{\text{sw}}(r_{12}), \tag{2.8b}$$

where ε' is a dimensionless parameter that we introduce so that we can vary the relative strength of the isotropic and anisotropic interactions. In Eqs. (2.8a) and (2.8b),

$$u_{\text{sw}}(r_{12}) = -\varepsilon\Theta(r_{12} - \sigma)\Theta(\lambda\sigma - r_{12}) \tag{2.9}$$

describes an attractive potential well and Θ is the Heaviside function; ε and $\lambda\sigma$ denote the depth and width of the attractive well, respectively. Finally, combining Eqs. (2.1), (2.2), and (2.8) we obtain the interaction potential

$$u(r_{12},\omega_1,\omega_2) = u_{\text{hs}}(r_{12}) + u_{\text{sw}}(r_{12})[1 + \varepsilon' P_2(x)], \tag{2.10}$$

which is identical to the one employed in an earlier DFT study by one of the present authors [29]. Throughout this work we fix $\varepsilon' = 0.4$.

Finally, we emphasize that liquid-crystalline behavior comes about through anisotropic attractions between a pair of molecules and not because of an interaction between anisotropic repulsive cores as it would in the case of rod-shaped or disklike particles. However, as far as the overall topology of phase diagrams is concerned it turns out that the disregard of an anisometric shape in favor of anisotropic attraction is irrelevant. To see this one should compare the phase diagram presented below in the field-free case with the one presented by Franco-Melgar [33] and Franco-Melgar *et al.* [34] who studied the phase behavior of hard spherocylinders in which the isotropic-nematic phase transition is solely driven by entropic rather than energetic features as in this work.

Nevertheless, it should be stressed that model systems in which the molecules possess an isotropic core with superimposed anisotropic attractions are computationally much more convenient than models with shape-anisometric cores both in computer simulations [30,35–38] and in classical DFT [29,39].

The present class of liquid-crystal model potentials has been used successfully to understand and explain structures in nematic colloidal suspensions [40] that were observed experimentally [41,42] but remained unexplained for nearly twenty years. Another example in which a model potential with an isotropic core and superimposed anisotropic interactions has been shown to be adequate is the investigation of defect topologies forming if colloidal particles are immersed in a nematic or smectic *A* carrier host phase [43]. The defect topologies observed theoretically [44] are in good qualitative agreement with experimental findings [45,46]. A third example is binary nematic mixtures of biaxial symmetry in which both pure compounds pertain to the present class of model systems [47].

The conclusion drawn from these earlier studies is that shape anisometry as well as anisotropic attraction between otherwise spherical molecules both capture the essential physics of a broad variety of liquid-crystalline systems.

B. External field

For a suitably chosen thermodynamic state the model liquid crystal introduced in the preceding section will form a nematic phase [29]. In this nematic phase the mesogens will align, at least to a certain degree, where the overall direction of alignment can be described by the nematic director $\hat{\boldsymbol{n}}$. However, without an external field the direction of $\hat{\boldsymbol{n}}$ is infinitely degenerate on the unit sphere. Normally, this is not necessarily a problem.

However, in this work, in which we want to use an external field to switch $\hat{\boldsymbol{n}}$ between its direction in a nonpolar nematic reference state and a polar-field-induced state, it seems sensible to have the same fixed direction of $\hat{\boldsymbol{n}}$ in that reference state. Thus, we are seeking to select one of the infinitely many possible directions of $\hat{\boldsymbol{n}}$ by applying a weak external field that, in addition, also preserves the "head-tail" symmetry (i.e., the indistinguishability of $\hat{\boldsymbol{n}}$ and $-\hat{\boldsymbol{n}}$) in the nematic phase.

This situation is akin to the one usually encountered in experiments. Experimentally, the liquid crystal is placed in a container. The walls of that container are capable of "anchoring" the mesogens in their immediate vicinity in specific ways. "Anchoring" refers to an energetic discrimination of certain orientations of the mesogens with respect to the container walls [48]. Experimentally, specific anchoring conditions can be realized by treating the container walls mechanically, chemically, or by exposing the liquid crystal to some external action.

For example, mechanical work can be applied by rubbing or polishing the walls, by exposing them to photolithographic relief, or by oblique evaporation of oxide films. Chemically, substrates can be modified through the deposition of surfactants or polymeric films. The former causes homeotropic anchoring of the mesogens whereas planar anchoring is realized by the latter modification. Finally, flow can be used to manipulate the anchoring of the mesogens at substrates which constitutes an example of external action. For more details the interested reader is referred to Sonin's book [49].

If the liquid crystal is in the isotropic phase only that portion in the immediate vicinity of the walls is affected by the specific anchoring scenario. However, in the nematic phase anchoring conditions are imprinted onto portions of the liquid crystal that are too far away from the container walls to directly interact with them. Nevertheless, these portions of the liquid crystal can exhibit the same ordering as those located in the vicinity of the walls. In other words, in the nematic phase we are dealing with long-range orientational order. We intend to mimic this experimental scenario by introducing an external field $\boldsymbol{H}_{\mathrm{n}} = H_{\mathrm{n}}\hat{\boldsymbol{H}}_{\mathrm{n}}$ that couples quadratically to the alignment tensor $\mathbf{Q}$ which is measure of nematic order in the liquid crystal [10]. Therefore, we introduce

$$u_{\mathrm{n}}(\omega) = -H_{\mathrm{n}}^2 \hat{\boldsymbol{H}}_{\mathrm{n}}^{\mathrm{T}} \mathbf{Q} \hat{\mathbf{H}}_{\mathrm{n}}, \tag{2.11}$$

where H_{n} is a coupling constant controlling the strength of the field $\boldsymbol{H}_{\mathrm{n}}$.

The field is acting in the z direction and therefore $\hat{\boldsymbol{H}}_{\mathrm{n}}^{\mathrm{T}} = (0, 0, 1)$ where T denotes the transpose. Thus, u_{n} tends to align a mesogen with the z axis. It should be perceived as the far field due to the anchoring of the mesogens at the container walls.

Components of the alignment tensor are given by

$$Q_{ij} = \frac{3}{2}\int d\omega\, \alpha(\omega) u_i(\omega) u_j(\omega) - \frac{1}{2}\delta_{ij}, \tag{2.12}$$

where δ_{ij} is the Kronecker symbol ($i, j = x, y, z$) and α is the orientation distribution function (odf). The latter is normalized according to

$$\int d\omega\, \alpha(\omega) = 1. \tag{2.13}$$

The second-rank tensor $\mathbf{Q}$ is real, symmetric, and traceless. It can be represented by a 3×3 matrix. In Eq. (2.12),

$$u_{\mathrm{x}}(\omega) = \sin\theta\cos\varphi = -\sqrt{\frac{8\pi}{3}}\,\mathrm{Re}\,\mathcal{Y}_{11}(\omega), \tag{2.14a}$$

$$u_{\mathrm{y}}(\omega) = \sin\theta\sin\varphi = -\sqrt{\frac{8\pi}{3}}\,\mathrm{Im}\,\mathcal{Y}_{11}(\omega), \tag{2.14b}$$

$$u_{\mathrm{z}}(\omega) = \cos\theta = \sqrt{\frac{4\pi}{3}}\,\mathcal{Y}_{10}(\omega), \tag{2.14c}$$

where Eq. (A.62) of Ref. [32] has also been invoked and Re and Im denote real and imaginary parts, respectively. From Eqs. (2.11) and (2.12) it is straightforward to verify that

$$u_{\mathrm{n}}(\omega) = -\frac{H_{\mathrm{n}}^2}{2}\left[3u_{\mathrm{z}}^2(\omega) - 1\right] = -H_{\mathrm{n}}'\mathcal{Y}_{20}(\omega) \tag{2.15}$$

and $H_{\mathrm{n}}' = H_{\mathrm{n}}^2\sqrt{4\pi/5}$ is a renormalized coupling constant where we lumped together the trivial prefactors arising from the definition of $\mathcal{Y}_{20}$ [32].

The focus of this work is on switching between a *nonpolar* nematic reference state and a *polar* nematic state. This requires the introduction of a second external field $\boldsymbol{H}_{\mathrm{p}}$. According to Mertelj and Lisjak [16] the coupling of polar order to this field should be linear. We assume that the field is orthogonal to $\boldsymbol{H}_{\mathrm{n}}$ and take $\hat{\boldsymbol{H}}_{\mathrm{p}}$ to point in the x direction, that is $\hat{\boldsymbol{H}}_{\mathrm{p}}^{\mathrm{T}} = (1, 0, 0)$. The external polar potential is then given by

$$u_{\mathrm{p}}(\omega) = H_{\mathrm{p}}\hat{\boldsymbol{H}}_{\mathrm{p}} \cdot \hat{\boldsymbol{u}}(\omega) = H_{\mathrm{p}}\sin\theta\cos\varphi = -H_{\mathrm{p}}'\,\mathrm{Re}\,\mathcal{Y}_{11}(\omega), \tag{2.16}$$

where $H_{\mathrm{p}}' \geqslant 0$ is a coupling constant that allows us to control the strength of the polar field. The unit vector $\hat{\boldsymbol{u}}$ in Eq. (2.16) can thus be interpreted as a magnetic moment carried by a mesogen. As before in Eq. (2.15) it is convenient to lump together all numerical prefactors from the definition of $\mathcal{Y}_{11}$ [see Eq. (A.62) of Ref. [32]] so that $H_{\mathrm{p}} \to H_{\mathrm{p}}'$. Combining now Eqs. (2.15) and (2.16) allows us to introduce the total external potential via

$$\begin{aligned} u_{\mathrm{ext}}(\omega) &= u_{\mathrm{n}}(\omega) + u_{\mathrm{p}}(\omega) \\ &= -H_{\mathrm{n}}'\mathcal{Y}_{20}(\omega) - H_{\mathrm{p}}'\,\mathrm{Re}\,\mathcal{Y}_{11}(\omega). \end{aligned} \tag{2.17}$$

However, it needs to be stressed that the model that we study attempts to mimic the experimental situation only implicitly. In experimental systems one focuses on suspensions of magnetic nanoplatelets in a liquid-crystalline host phase. Assuming that the liquid-crystal molecules are sufficiently strongly anchored at the surface of the nanoplatelets, the nematic director can be rotated through the response of the

nanoplatelets to an external magnetic field. To avoid the additional effort to treat a binary mixture within the framework of the present approach we simply add another (independent) degree of freedom to our liquid-crystal molecules capable of responding to the external field $\boldsymbol{H}_{\mathrm{p}}$. As we argue in Sec. VII, to treat the ferromagnetic nematic suspension as an *effective* single-component liquid crystal is actually advantageous from a theoretical perspective.

III. APPROXIMATE FREE-ENERGY FUNCTIONAL

A. Preliminary remarks

For the model introduced in Sec. II we are ultimately interested in thermodynamic equilibrium states under various conditions characterized by, for example, temperature T or chemical potential μ, but also for various coupling strengths H_{n}' and H_{p}'. These thermodynamic equilibrium states correspond to minima of the grand-potential functional given by the expression

$$\Omega[\rho(\boldsymbol{r},\omega)] = \mathcal{F}[\rho(\boldsymbol{r},\omega)] + \iint d\boldsymbol{r}\, d\omega\, \rho(\boldsymbol{r},\omega) u_{\mathrm{ext}}(\omega) - \mu \iint d\boldsymbol{r}\, d\omega \rho(\boldsymbol{r},\omega), \tag{3.1}$$

where ρ is the generic singlet distribution function [32] and $\mathcal{F}$ is the free-energy functional. The second term on the right-hand side of Eq. (3.1) represents the free-energy contribution due to u_{ext} [see Eq. (2.17)]. Thus, Ω can be perceived as a generalized Legendre transform of $\mathcal{F}$.

We decompose $\mathcal{F}$ into an ideal-gas contribution $\mathcal{F}_{\mathrm{id}}$ and an excess contribution $\mathcal{F}^{\mathrm{ex}}$ which we define through the expression

$$\mathcal{F}^{\mathrm{ex}}[\rho(\boldsymbol{r},\omega)] \equiv \mathcal{F}[\rho(\boldsymbol{r},\omega)] - \mathcal{F}_{\mathrm{id}}[\rho(\boldsymbol{r},\omega)]. \tag{3.2}$$

Because of this definition, the functional $\mathcal{F}^{\mathrm{ex}}$ accounts for all intrinsic free-energy contributions. An explicit expression for $\mathcal{F}_{\mathrm{id}}$ is given in Eq. (3.15) below.

B. Excess free-energy functional

At this stage one realizes that it will not be possible to derive an *exact* expression for $\mathcal{F}^{\mathrm{ex}}$ on account of the relative complexity of our model system. The best one can be hoping for is to develop an *approximate* but sufficiently accurate expression for $\mathcal{F}^{\mathrm{ex}}$.

To develop such an expression we begin by decomposing u in Eq. (2.10) into a contribution u_0 of a reference system and a perturbation u_1 according to $u = u_0 + u_1$. The choice of the reference system and that of the perturbation is by no means unique. Therefore, we assume that the unweighted orientational average of u_1 satisfies

$$\langle u_1(r_{12},\omega_1,\omega_2)\rangle_{\omega_1,\omega_2} = \frac{1}{4\pi}\iint d\omega_1\, d\omega_2\, u_1(r_{12},\omega_1,\omega_2) = 0. \tag{3.3}$$

An inspection of Eq. (2.10) immediately suggests that $u_1 = u_{\mathrm{aniso}}$ owing to the "multipolelike" character [50] of u_{aniso} [see Eq. (3.3)]. To see that u_{aniso} satisfies Eq. (3.3) one realizes from Eq. (2.7b) and the addition theorem for spherical harmonics [see Eq. (A.33) of Ref. 32] that

$$u_{\mathrm{aniso}}(r_{12},\omega_1,\omega_2) \propto P_2(x) = \frac{4\pi}{5}\sum_{m=-2}^{2} \mathcal{Y}_{2m}^{*}(\omega_1)\mathcal{Y}_{2m}(\omega_2). \tag{3.4}$$

Because of this relationship and using Eq. (A.38) of Ref. [32] it is apparent that u_{aniso} satisfies Eq. (3.3).

From this discussion and Eq. (2.10) it is then clear that

$$u_0(r_{12}) = u(r_{12},\omega_1,\omega_2) - u_1(r_{12},\omega_1,\omega_2) = u_{\mathrm{iso}}(r_{12}) \tag{3.5}$$

describes the interaction of particles in the reference system. Because of the decomposition of u into u_0 and u_1 we are now ready to develop an explicit expression for the intrinsic free-energy functional in Eq. (3.1). Therefore, we introduce

$$u(r_{12},\omega_1,\omega_2;\xi) = u_0(r_{12}) + \xi u_1(r_{12},\omega_1,\omega_2), \tag{3.6}$$

where $0 \leqslant \xi \leqslant 1$ is a dimensionless parameter that allows us to specify a linear path of integration along which we can switch continuously between the reference system ($\xi = 0$) and the system of interest ($\xi = 1$).

Because of Eq. (3.6), $\mathcal{F}^{\mathrm{ex}}$ becomes a function of ξ. As detailed in Ref. [29] one can then take recourse to thermodynamic integration and introduce a change in the excess free energy functional,

$$\begin{aligned}\Delta\mathcal{F}^{\mathrm{ex}} &= \mathcal{F}_1^{\mathrm{ex}} - \mathcal{F}_0^{\mathrm{ex}} \\ &= \frac{1}{2}\int_0^1 d\xi \iint d\boldsymbol{r}_1 d\boldsymbol{r}_2 \iint d\omega_1 d\omega_2 u_1(r_{12},\omega_1,\omega_2) \\ &\quad\times \rho(\boldsymbol{r}_1,\omega_1)\rho(\boldsymbol{r}_2,\omega_2) g(\boldsymbol{r}_1,\boldsymbol{r}_2,\omega_1,\omega_2;\xi),\end{aligned} \tag{3.7}$$

where $\mathcal{F}_0^{\mathrm{ex}}$ and $\mathcal{F}_1^{\mathrm{ex}}$ are the excess free-energy functional of the reference system and that of the system of interest, respectively. In Eq. (3.7), g denotes the orientation-dependent pair correlation function which depends on the coupling parameter ξ. In other words, for each value of ξ a different pair correlation function is needed which consequently requires a suitable parametrization of g [29].

Such a parametrization is possible if one expands the so-called cavity correlation function in terms of ξ as explained in detail elsewhere [29]. To leading order this expansion gives

$$g(\boldsymbol{r}_1,\boldsymbol{r}_2,\omega_1,\omega_2;\xi) = g_0(r_{12})\exp[-\beta\xi u_1(r_{12},\omega_1,\omega_2)], \tag{3.8}$$

where g_0 is the radial pair correlation function of the reference system.

The previous expression constitutes the augmented modified mean-field (AMMF) approximation [29]. In essence, the AMMF approximation assumes that the short-range positional structure of the liquid crystal is solely determined by the isotropic interactions between the mesogenic cores; the anisotropic interactions enter the physical picture only at the level of the second virial coefficient.

With Eq. (3.8) it is now possible to carry out the integration over the coupling constant in Eq. (3.7) analytically which

gives

$$\beta\Delta\mathcal{F}^{\rm ex} = -\frac{1}{2}\iint d\boldsymbol{r}_1 d\boldsymbol{r}_2 g_0(r_{12}) \times \iint d\omega_1 d\omega_2 f(r_{12},\omega_1,\omega_2) \times \rho(\boldsymbol{r}_1,\omega_1)\rho(\boldsymbol{r}_2,\omega_2), \tag{3.9}$$

where

$$f(r_{12},\omega_1,\omega_2) = \exp[-\beta u_{\rm aniso}(r_{12},\omega_1,\omega_2)] - 1 \tag{3.10}$$

is the orientation-dependent Mayer f function and $\beta = 1/k_{\rm B}T$ ($k_{\rm B}$ is Boltzmann's constant). For mesogens of uniaxial symmetry f can be expanded in terms of rotational invariants (see Sec. A.4.2 of Ref. [32]) according to

$$f(r_{12},\omega_1,\omega_2) = \sum_{l_1 l_2 l} f_{l_1 l_2 l}(r_{12})\Phi_{l_1 l_2 l}(\omega_1,\omega_2,\omega). \tag{3.11}$$

Because we are dealing with a homogeneous bulk system we decompose the generic singlet distribution functions in Eq. (3.9) according to

$$\rho(\boldsymbol{r},\omega) = \rho\alpha(\omega), \tag{3.12}$$

where ρ on the right-hand side is the number density. Putting all this together, we can rewrite Eq. (3.9) as

$$\frac{\beta\Delta\mathcal{F}^{\rm ex}}{V} \equiv \beta\Delta f^{\rm ex} = \rho^2 \sum_{lm} \alpha_{lm}\alpha_{l\underline{m}} u_{lm}(\rho). \tag{3.13}$$

The energy parameters $\{u_{lm}\}$ in Eq. (3.13) are given by

$$u_{lm}(\rho) = -\frac{(-1)^{l+m}\sqrt{\pi}}{\sqrt{2l+1}} \int_0^\infty dr_{12}\, r_{12}^2\, g_0(r_{12}) f_{ll0}(r_{12}), \tag{3.14}$$

where the density dependence arises through g_0. Explicit expressions for elements of the set $\{f_{ll0}\}$ are given in Appendix C of Ref. [29]. Details of the integration over orientations in Eq. (3.9) leading to Eq. (3.13) are discussed in Appendix B.

To arrive at Eq. (3.13), we transformed variables $\boldsymbol{r}_1 \to \boldsymbol{r}_1' = \boldsymbol{r}_1$, $\boldsymbol{r}_2 \to \boldsymbol{r}_2' = \boldsymbol{r}_{12}$, performed the one trivial integration over $d\boldsymbol{r}_1'$, and used spherical coordinates where $d\boldsymbol{r}_{12} = r_{12}^2 dr_{12} d\omega$. At this stage, the reader should realize that $\Delta\mathcal{F}^{\rm ex}$ has become a *function* of ρ but remains a *functional* of α because of Eq. (3.12).

Finally, on account of the approximation introduced in Eq. (3.12) we can express the ideal-gas contribution as

$$\frac{\beta\mathcal{F}_{\rm id}}{V} \equiv \beta f_{\rm id} = \rho[\ln(\rho\Lambda^5 m/I) - 1] + \rho\int d\omega\, \alpha(\omega)\ln[4\pi\alpha(\omega)], \tag{3.15}$$

which is a *function* of ρ and a *functional* of α as well. The first term on the far right-hand side of Eq. (3.15) arises from the kinetic energy of the mesogens; the second one accounts for the entropic loss if the liquid crystal undergoes a transition from a disordered to an ordered phase. The extra factor of 4π in the argument of the logarithmic function is included to make sure the the second term on the right-hand side of Eq. (3.15) vanishes in the isotropic phase for which $\alpha = \frac{1}{4\pi}$ because of Eq. (2.13).

C. Free energy of the reference system

Turning now to the free energy of the reference system $\mathcal{F}_0^{\rm ex}$, this consists of two contributions. The first of these is the free energy due to the hard-core repulsion [see Eq. (2.2)]. Because the system is homogeneous [see Eqs. (2.15) and (2.16)] we can employ the Carnahan-Starling equation of state [51] from which one obtains the free-energy density of the hard-sphere fluid [52] as

$$\frac{\beta\mathcal{F}_{\rm hs}}{V} \equiv \beta f_{\rm hs} = \rho\frac{4\eta - 3\eta^2}{(1-\eta)^2}. \tag{3.16}$$

In Eq. (3.16), $\eta \equiv \frac{\pi}{6}\rho\sigma^3$ is the packing fraction of the hard spheres at density ρ.

The second contribution to $\mathcal{F}_0^{\rm ex}$ comes from the attractive trough of the square-well potential [see Eq. (2.9)]. We treat this contribution within thermodynamic perturbation theory *á la* Barker and Henderson [53] or Zwanzig [54,55]. To leading order this approach gives

$$\frac{\beta\mathcal{F}_{\rm sw}}{V} \equiv \beta f_{\rm sw} = 2\pi\beta\rho^2 \int_0^\infty dr_{12}\, r_{12}^2 u_{\rm sw}(r_{12}) g_{\rm hs}(r_{12}), \tag{3.17}$$

where $g_{\rm hs}$ is the radial pair correlation function of a hard-sphere fluid.

The integrand in this expression is negative semidefinite because $u_{\rm sw} \leqslant 0$ and $g_{\rm hs} \geqslant 0$ regardless of r_{12}. This allows us to invoke the first mean-value theorem for definite integrals so that the previous expression for $f_{\rm sw}$ can be rewritten as [56]

$$\beta f_{\rm sw} = 2\pi\beta\rho^2 g_{\rm hs}^{\rm c}(\eta_{\rm eff}) \int_0^\infty dr_{12}\, r_{12}^2 u_{\rm sw}(r_{12}) \simeq -\frac{2\pi}{3}\beta\varepsilon\rho^2\sigma^3 g_{\rm hs}^{\rm c}(\eta_{\rm eff})(\lambda^3 - 1), \tag{3.18}$$

where $g_{\rm hs}^{\rm c} = \lim_{r_{12}\to\sigma^+} g_{\rm hs}$ is the contact value of the radial pair correlation function.

The parameter $\eta_{\rm eff}$ is an *effective* hard-sphere packing fraction. It can be parametrized in terms of η. The parametrization is known for a great many potentials [56] (for the square-well potential, see Eqs. (26) and (27) of Ref. [29]).

One can then invoke the contact-value theorem for the pressure of a hard-sphere fluid (see Eq. (2.5.26) of Ref. [52]) and combine it with the Carnahan-Starling equation of state [51] to obtain

$$g_{\rm hs}^{\rm c}(\eta_{\rm eff}) = \frac{1 - \eta_{\rm eff}/2}{(1-\eta_{\rm eff})^3}. \tag{3.19}$$

Applying a similar perturbative treatment then allows us to rewrite Eq. (3.14) as

$$u_{lm}(\rho) = -\frac{(-1)^{l+m}\sqrt{\pi}}{\sqrt{2l+1}} g_{\rm hs}^{\rm c}(\eta_{\rm eff}) \int_0^\infty dr_{12}\, r_{12}^2\, f_{ll0}(r_{12}). \tag{3.20}$$

Because m enters Eqs. (3.14) and (3.20) as a trivial factor, we have

$$u_{lm}(\rho) = (-1)^{|m|+1}(2l+1)u_l(\rho), \tag{3.21}$$

where explicit expressions for the first few members of the set $\{u_l\}$ are given in Eqs. (101a)–(101c) of Ref. [29].

Hence, from Eqs. (3.16) and (3.18) together with Eq. (3.19) we are in a position to calculate the excess free energy of the isotropic reference system from

$$\mathcal{F}_0^{\rm ex}(\rho) = \mathcal{F}_{\rm hs}(\rho) + \mathcal{F}_{\rm sw}(\rho), \tag{3.22}$$

which turns out to be only a *function* of ρ (and not a *functional*) because of Eq. (3.12) and because the reference system consists of spherically symmetric particles [see Eq. (3.6)].

IV. MINIMIZING THE GRAND-POTENTIAL FUNCTIONAL

Collecting the various free-energy contributions given in Eqs. (3.13), (3.15), (3.16), and (3.18) permits us to construct the approximate functional for Ω that we are now seeking to minimize. It can be written as

$$\frac{\beta\Omega[\rho,\alpha(\omega)]}{V} = \beta f_{\rm sw} + \beta f_{\rm hs} + \beta f_{\rm id} + \rho^2 \sum_{lm} \alpha_{lm}\alpha_{l\underline{m}}u_{lm} + \beta\rho\int d\omega\,\alpha(\omega)u_{\rm ext}(\omega) - \beta\mu\rho, \tag{4.1}$$

where we dropped ρ as an argument of $f_{\rm sw}$, $f_{\rm hs}$, $f_{\rm id}$, and $\{u_{lm}\}$ on the right-hand side to ease the notational burden. Using this expression for Ω allows us to identify thermodynamically stable states and also permits us to study phase coexistence.

A. Thermodynamically stable states

Generally speaking, thermodynamically stable states correspond to minima of the approximate grand-potential functional given in Eq. (4.1). Hence, we are seeking simultaneous solutions of the equations

$$\left(\frac{\partial\,\Omega}{\partial\,\rho}\right) = 0, \tag{4.2a}$$

$$\left(\frac{\delta\Omega}{\delta\alpha(\omega)}\right) = \chi(T,\rho), \tag{4.2b}$$

where χ is a Lagrangian multiplier introduced to make sure that the functional derivative on the left-hand side of Eq. (4.2b) automatically satisfies the normalization condition in Eq. (2.13). Using Eq. (4.2a) it is straightforward to verify that

$$0 = \beta\mu_{\rm sw} + \beta\mu_{\rm hs} + \beta\mu_{\rm id} + \sum_{lm}\alpha_{lm}\alpha_{l\underline{m}}\left[2\rho u_{lm}(\rho) + \rho^2\frac{du_{lm}(\rho)}{d\rho}\right] + \beta\int d\omega\,\alpha(\omega)u_{\rm ext}(\omega) - \beta\mu, \tag{4.3}$$

where Eq. (3.13) has also been utilized and $\mu_\bullet = \partial f_\bullet/\partial\rho$. Solving Eq. (4.3) for $\beta\mu$ and replacing this term in Eq. (4.1) then gives

$$\frac{\beta\Omega[\rho,\alpha(\omega)]}{V} = -\beta P = \beta P_{\rm CS} - \beta P_{\rm sw} - \sum_{lm}\alpha_{lm}\alpha_{l\underline{m}}\left[\rho^2 u_{lm}(\rho) + \rho^3\frac{du_{lm}(\rho)}{d\rho}\right], \tag{4.4}$$

where P is the total pressure and $P_{\rm CS}$ is given by the Carnahan-Starling equation of state [51] (see also Eq. (3.9.17) of Ref. [52]); $P_{\rm sw}$ is the pressure contribution from the attractive square well. An explicit expression for the latter is given in Eq. (61b) of Ref. [29].

To solve Eq. (4.2b) we first need to replace α_{lm} and $\alpha_{l\underline{m}}$ in the fourth term on the right-hand side of Eq. (4.1). We notice from Eq. (B2) and because the spherical harmonics form a complete set of orthonormal basis functions that

$$\alpha_{lm} = \int d\omega\,\alpha(\omega)\mathcal{Y}_{lm}^*(\omega). \tag{4.5}$$

We note in passing that because of Eq. (A.38) in the book by Gray and Gubbins [32] all expansion coefficients α_{lm} vanish in the isotropic phase except for $\alpha_{00} = 1/\sqrt{4\pi}$ because of Eq. (2.13).

Reminding ourselves that $f_{\rm id}$ is a functional of α we can then perform the functional derivative in Eq. (4.2b). Solving the resulting expression for the odf we obtain the expression

$$\alpha(\omega) = \frac{1}{4\pi}\exp\left[\frac{\chi(T,\rho)-\rho}{\rho}\right]\Psi(\omega) = \frac{1}{4\pi}\frac{\Psi(\omega)}{\langle\Psi(\omega)\rangle_\omega}, \tag{4.6}$$

where the expression on the far right-hand side follows with the aid of Eq. (2.13). In the previous expression the *unnormalized* odf is given by

$$\Psi(\omega) = \exp\left[-2\rho\sum_{\substack{l>0\\ m}} u_{lm}(\rho)\alpha_{lm}\mathcal{Y}_{l\underline{m}}^*(\omega) - \beta u_{\rm ext}(\omega)\right] \times \exp\left[-\frac{\rho u_{00}(\rho)}{2\pi}\right] \tag{4.7}$$

and

$$\langle\Psi(\omega)\rangle_\omega = \frac{1}{4\pi}\int d\omega\,\Psi(\omega) \tag{4.8}$$

is its unweighted average over orientations.

The second term on the right-hand side of Eq. (4.7) accounts for the isotropic ($l = m = 0$) contribution. This contribution cancels between numerator and denominator of the expression on the far right-hand side of Eq. (4.6). Moreover, because $u_{lm} \propto f_{l|0}$ [see Eq. (3.20)] and the analysis in Appendix C of Ref. [29] reveals that the set $\{f_{l|0}\}$ comprises only coefficients for even l, the sum over l in the first term on the right-hand side of Eq. (4.7) does, too. This is a direct consequence of the orientation dependence of $u_{\rm aniso}$ in Eq. (2.7b).

Finally, we note that quantities such as $\sum_{lm}\alpha_{lm}\alpha_{l\underline{m}}$ [see Eq. (4.4)] and $\sum_{lm}\alpha_{lm}\mathcal{Y}_{l\underline{m}}$ [see Eq. (4.7)] are real as they must be. This is a consequence of Eq. (A.3) of the book by Gray and Gubbins [32] which is satisfied by both $\mathcal{Y}_{l\underline{m}}$ and $\alpha_{l\underline{m}}$ in conjunction with the summation over m in Eqs. (4.4) and (4.7).

B. Coexisting phases

For any thermodynamic state point characterized by its temperature T and density ρ we are now in a position to calculate the odf from Eq. (4.6). With this odf we can compute the corresponding set of expansion coefficients $\{\alpha_{lm}\}$ from

Eq. (4.5). Thus, employing Eq. (4.4) we can obtain the grand-potential density for the given T and ρ.

Unfortunately, we have no way of telling beforehand whether this value of Ω corresponds to a true thermodynamic equilibrium state point, that is whether or not this particular combination of T and ρ is associated with a thermodynamically metastable or stable situation [57]. However, we can easily discriminate between these two situations on the basis of the full phase diagram.

The latter can be determined by assuming that a pair of phases $'$ and $''$ exists, satisfying the constraints

$$T' = T'', \tag{4.9a}$$

$$P' = P'', \tag{4.9b}$$

$$\mu' = \mu''. \tag{4.9c}$$

Henceforth, we will also assume that, without loss of generality, $\rho' \leqslant \rho''$; the equal sign applies at the critical point at which the gas and liquid phases become indistinguishable.

The first constraint given in Eq. (4.9a) is implemented by simply setting $T' = T'' = T$ as an input parameter to our minimization procedure. A comparison between Eqs. (4.4) and (4.9b) then reveals that the second constraint gives rise to a nonlinear algebraic equation of the general form,

$$s_1(\rho', \rho'', \{\alpha'_{lm}\}, \{\alpha''_{lm}\}) = 0. \tag{4.10}$$

An explicit expression for s_1 can easily be derived from Eq. (4.4) keeping in mind that $\alpha_{00} = 1/\sqrt{4\pi}$.

In Eq. (4.10), the function depends on the set of parameters $\{\alpha'_{lm}\}$ for the lower-density phase $'$. If this phase is a gas (G), clearly no ordered phase can form. However, the mesogens will exhibit some residual order because of the presence of u_{ext}. That order needs to be accounted for. Without u_{ext}, the G phase would self-evidently be isotropic.

The third constraint eventually leads to a second nonlinear algebraic equation

$$s_2(\rho', \rho'', \{\alpha'_{lm}\}, \{\alpha''_{lm}\}) = 0. \tag{4.11}$$

It needs to be solved simultaneously with Eq. (4.10). The derivation of s_2 is slightly more involved. From Eq. (3.15) it is straightforward to derive an expression for $\beta\mu_{\text{id}}$. It contains the integral $\int d\omega\, \alpha \ln(4\pi\alpha)$. The logarithmic term can then be replaced with the aid of Eqs. (4.6) and (4.7) keeping in mind the normalization of α [see Eq. (2.13)]. We can now solve Eq. (4.3) for $\beta\mu$, replace in the resulting expression $\beta\mu_{\text{id}}$ by the previously derived equation, and apply Eq. (4.9c) to obtain an explicit form for Eq. (4.11).

Nevertheless, it should be clear that the simultaneous solution of Eqs. (4.10) and (4.11) requires the sets $\{\alpha'_{lm}\}$ and $\{\alpha''_{lm}\}$ obtained at thermodynamic equilibrium. To compute these parameters we solve the consistency equations

$$t'^{,''}_{lm} = \alpha'^{,''}_{lm} - \int d\omega\, \alpha'^{,''}(\omega) \mathcal{Y}^*_{lm}(\omega) = 0, \tag{4.12}$$

alongside Eqs. (4.10) and (4.11) where Eq. (4.5) has also been employed and $\alpha'^{,''}$ is computed from the far right-hand side of Eq. (4.6).

The reader should notice that for each l there are $2l + 1$ additional equations of the form given in Eq. (4.12) that we need to solve for the phases $'$ and $''$. Hence, the computational effort increases substantially with l even for relatively small values. To limit the computational effort we therefore restrict ourselves to $l = 2$ henceforth.

V. MEASURES OF ORIENTATIONAL ORDER

We now turn to a discussion of key properties that we intend to compute in order to investigate the formation of ordered phases at and off phase coexistence. The most important one is the alignment tensor already introduced in Eq. (2.12). Using Eqs. (2.14) and (4.5) as well as Eqs. (A.3) and (A.36) of Ref. [32] one can show that

$$\mathbf{Q} = \sqrt{\frac{6\pi}{5}} \begin{pmatrix} \operatorname{Re}\alpha_{22} - \frac{\alpha_{20}}{\sqrt{6}} & -\operatorname{Im}\alpha_{22} & -\operatorname{Re}\alpha_{21} \\ -\operatorname{Im}\alpha_{22} & -\operatorname{Re}\alpha_{22} - \frac{\alpha_{20}}{\sqrt{6}} & \operatorname{Im}\alpha_{21} \\ -\operatorname{Re}\alpha_{21} & \operatorname{Im}\alpha_{21} & \sqrt{\frac{2}{3}}\alpha_{20} \end{pmatrix}. \tag{5.1}$$

The alignment tensor satisfies the eigenvalue equation

$$\mathbf{Q}\,\hat{\boldsymbol{n}}_{\pm,0} = \lambda_{\pm,0}\,\hat{\boldsymbol{n}}_{\pm,0}, \tag{5.2}$$

where $\{\lambda_{\pm,0}\}$ are the three eigenvalues and $\{\hat{\boldsymbol{n}}_{\pm,0}\}$ are the associated eigenvectors. Equation (5.2) is solved numerically using Jacobi's transformation [58]. We follow Eppenga and Frenkel [59] and define the nematic order parameter S via

$$S = \lambda_+, \tag{5.3}$$

where λ_+ is the largest eigenvalue of the alignment tensor. The nematic director is then given as $\hat{\boldsymbol{n}} = \hat{\boldsymbol{n}}_+$. The eigenvalues can thus be ordered through the inequality $\lambda_- \leqslant \lambda_0 < \lambda_+$ where the equality holds in the absence of biaxial symmetry. Because $\operatorname{Tr}\mathbf{Q} = 0$, $0 \leqslant S \leqslant 1$ [59] (see also Appendix C).

We now want to derive explicit expressions for the three eigenvalues of $\mathbf{Q}$ in terms of the expansion coefficients of the odf. To that end we remind ourselves that because of the presence of the two external potentials u_{n} and u_{p} and if our system is ordered, $\hat{\boldsymbol{n}}$ will be pointing in some direction in the x-z plane. Because the eigenspace of $\mathbf{Q}$ is spanned by three pairwise orthogonal vectors, one of the two remaining eigenvectors must also lie in the x-z plane and the third one must coincide with $\hat{\boldsymbol{e}}_{\text{y}}$.

Inserting in Eq. (5.2), $\hat{\boldsymbol{e}}_{\text{y}}$ as one of the eigenvectors of $\mathbf{Q}$, one immediately realizes that $\hat{\boldsymbol{e}}_{\text{y}}$ can only be an eigenvector of $\mathbf{Q}$ if one assumes that in Eq. (5.1), $\operatorname{Im}\alpha_{21} = \operatorname{Im}\alpha_{22} = 0$. Applying this rationale, the alignment tensor becomes

$$\mathbf{Q} = \sqrt{\frac{6\pi}{5}} \begin{pmatrix} \operatorname{Re}\alpha_{22} - \frac{\alpha_{20}}{\sqrt{6}} & 0 & -\operatorname{Re}\alpha_{21} \\ 0 & -\operatorname{Re}\alpha_{22} - \frac{\alpha_{20}}{\sqrt{6}} & 0 \\ -\operatorname{Re}\alpha_{21} & 0 & \sqrt{\frac{2}{3}}\alpha_{20} \end{pmatrix}. \tag{5.4}$$

The secular equation corresponding to Eq. (5.4) is easy to solve and gives the set of eigenvalues of $\mathbf{Q}$ as

$$\lambda_- = -\sqrt{\frac{6\pi}{5}}\left(\operatorname{Re}\alpha_{22} + \frac{\alpha_{20}}{\sqrt{6}}\right), \tag{5.5a}$$

$$\lambda_0 = \sqrt{\frac{6\pi}{5}}\left[\frac{1}{2}\left(\operatorname{Re}\alpha_{22} + \frac{\alpha_{20}}{\sqrt{6}}\right) - \frac{\Delta}{2}\right], \tag{5.5b}$$

$$\lambda_+ = \sqrt{\frac{6\pi}{5}}\left[\frac{1}{2}\left(\operatorname{Re}\alpha_{22} + \frac{\alpha_{20}}{\sqrt{6}}\right) + \frac{\Delta}{2}\right], \tag{5.5c}$$

where

$$\Delta = \sqrt{\left(\mathrm{Re}\,\alpha_{22} - \sqrt{\frac{3}{2}}\alpha_{20}\right)^2 + (2\,\mathrm{Re}\,\alpha_{21})^2}. \tag{5.6}$$

The expansion coefficients α_{20}, $\mathrm{Re}\,\alpha_{21}$, and $\mathrm{Re}\,\alpha_{22}$ can be obtained with the aid of Eq. (4.5).

In Appendix C we consider an idealized odf describing a perfectly ordered nematic phase. In this case, Eq. (5.2) can be solved analytically. The results of these considerations indicate that $S = 1$ is always obtained regardless of the direction of $\hat{\boldsymbol{n}}$ in the -$x - z$ plane.

If the contribution proportional to $\boldsymbol{H}_\mathrm{p}$ dominates the structure of the nematic liquid crystal, this nematic phase becomes polar. In this case, S is insufficient to fully characterize the degree of order in the polar nematic phase. Therefore, we follow Gramzow and Klapp [60] and introduce components of the polarization vector $\widetilde{P}$ via

$$\widetilde{P}_\mathrm{x} = \int d\omega\, \alpha(\omega) u_\mathrm{x}(\omega) = -\sqrt{\frac{8\pi}{3}}\,\mathrm{Re}\,\alpha_{11}, \tag{5.7a}$$

$$\widetilde{P}_\mathrm{y} = \int d\omega\, \alpha(\omega) u_\mathrm{y}(\omega) = \sqrt{\frac{8\pi}{3}}\,\mathrm{Im}\,\alpha_{11}, \tag{5.7b}$$

$$\widetilde{P}_\mathrm{z} = \int d\omega\, \alpha(\omega) u_\mathrm{z}(\omega) = \sqrt{\frac{4\pi}{3}}\alpha_{10}, \tag{5.7c}$$

where the polarization is defined as

$$P = \sqrt{\widetilde{P}_\mathrm{x}^2 + \widetilde{P}_\mathrm{y}^2 + \widetilde{P}_\mathrm{z}^2}. \tag{5.8}$$

This allows us to compute the unit polarization vector via

$$\hat{\boldsymbol{P}} = \frac{\widetilde{\boldsymbol{P}}}{P} = P_\mathrm{x}\hat{\boldsymbol{e}}_\mathrm{x} + P_\mathrm{y}\hat{\boldsymbol{e}}_\mathrm{y} + P_\mathrm{z}\hat{\boldsymbol{e}}_\mathrm{z}. \tag{5.9}$$

To gain deeper insight into the structure of the liquid crystal in the presence of u_ext we also consider the odf. From Eqs. (4.6) and (4.7) the odf can easily be obtained. However, to enhance the clarity of its visualization, we employ a rotated coordinate system. The protocol for this rotation is very similar to that described in Appendix A of the paper by Skutnik *et al.* [47].

We define an axis of rotation through the relationship

$$\widetilde{\boldsymbol{k}}' = \frac{\hat{\boldsymbol{n}} \times \hat{\boldsymbol{e}}_\mathrm{y}}{|\hat{\boldsymbol{n}} \times \hat{\boldsymbol{e}}_\mathrm{y}|}, \tag{5.10}$$

where the angle of rotation is given by $\cos\phi' = \hat{\boldsymbol{n}} \cdot \hat{\boldsymbol{e}}_\mathrm{y}$. It is then possible to construct a rotation tensor through the expression [47]

$$\mathbf{R}(k', \phi') = \mathbf{K}\sin\phi' + \mathbf{1}\cos\phi', \tag{5.11}$$

where $\mathbf{1}$ is the unit tensor and the traceless, skew-symmetric, second-rank tensor $\mathbf{K}$ is given by

$$\mathbf{K} = \begin{pmatrix} 0 & -k_3' & k_2' \\ k_3' & 0 & -k_1' \\ -k_2' & k_1 & 0 \end{pmatrix} \tag{5.12}$$

and $\{k_i'\}$ are components of the vector $\widetilde{\boldsymbol{k}}'$.

To make sure that all three eigenvectors of $\mathbf{Q}$ coincide with an axis of the rotated coordinate system, a second rotation is required. To that end we define a second axis of rotation $\hat{\boldsymbol{k}}''$ through the expression given in Eq. (5.10) replacing, however, $\hat{\boldsymbol{n}}$ and $\hat{\boldsymbol{e}}_\mathrm{y}$ by $\hat{\boldsymbol{n}}_0$ and $\hat{\boldsymbol{e}}_\mathrm{x}$, respectively. Together with a second angle of rotation defined similarly through the relation $\cos\phi'' = \hat{\boldsymbol{n}}_0 \cdot \hat{\boldsymbol{e}}_\mathrm{x}$ we then replace in Eqs. (5.11) and (5.12) the respective variables by ϕ'' and components of $\hat{\boldsymbol{k}}''$. This gives a second rotation tensor $\mathbf{R}$. The full rotation is then effected by the joint tensor

$$\mathbf{R} = \mathbf{R}(\hat{\boldsymbol{k}}', \phi')\mathbf{R}(\hat{\boldsymbol{k}}'', \phi''). \tag{5.13}$$

We can now compute new angles $\widetilde{\theta}$ and $\widetilde{\varphi}$ from the expression

$$\hat{\boldsymbol{n}}_\mathrm{rot} = \begin{pmatrix} \sin\widetilde{\theta}\cos\widetilde{\varphi} \\ \sin\widetilde{\theta}\sin\widetilde{\varphi} \\ \cos\widetilde{\theta} \end{pmatrix} = \mathbf{R}\hat{\boldsymbol{n}}, \tag{5.14}$$

where some precaution needs to be taken to make sure that the azimuthal angle $\widetilde{\varphi}$ is computed so that $\hat{\boldsymbol{n}}_\mathrm{rot}$ is given for the correct quadrant of the $\widetilde{x}$-$\widetilde{y}$ plane of the rotated coordinate system.

Note that if the system would exhibit perfect nematic order, $\hat{\boldsymbol{n}}_\mathrm{rot}^\mathrm{T} = (0, \pm 1, 0)$ and one would therefore expect α to exhibit two very sharp maxima at $\widetilde{\theta} = \frac{\pi}{2}$ and $\widetilde{\varphi} = \pm\frac{\pi}{2}$. This is because in the nematic phase, $\hat{\boldsymbol{n}}_\mathrm{rot}$ and $-\hat{\boldsymbol{n}}_\mathrm{rot}$ describe the same physical situation.

VI. RESULTS

Henceforth, we give all physical quantities in the customary dimensionless (i.e., "reduced") units as listed in Appendix B of the book by Allen and Tildesley [61]. For example, energy is expressed in units of the depth ε of the attractive trough, length in units of the hard-core diameter σ, and temperature in units of ε/k_B.

A. Phase behavior and order without a polar field

Throughout this work we use weak nematic fields $\boldsymbol{H}_\mathrm{n}$ by setting the coupling constant H_n' to small values. These small values should be viewed as a compromise. On the one hand, H_n' is small enough to make sure that the formation of a nematic liquid is mostly due to the choice of a particular thermodynamic state. On the other hand, H_n' is large enough to guarantee that for $\hat{\boldsymbol{H}}_\mathrm{p} = \mathbf{0}$, $\hat{\boldsymbol{n}} = \hat{\boldsymbol{e}}_\mathrm{z}$ where $\hat{\boldsymbol{e}}_\mathrm{z}^\mathrm{T} = (0, 0, 1)$ is pointing in the z direction of a space-fixed Cartesian coordinate system.

At this point it needs to be emphasized that if we choose an unphysical starting configuration characterized by $\hat{\boldsymbol{n}} \cdot \hat{\boldsymbol{e}}_\mathrm{z} = 0$, the iterative solution of Eqs. (4.10) and (4.11) together with Eq. (4.12) gives solutions that, once convergence has been achieved, are characterized by $\hat{\boldsymbol{n}} \cdot \hat{\boldsymbol{e}}_\mathrm{z} = 1$. This consistency relation is also satisfied off coexistence.

In Fig. 1 we present a plot of the phase diagram in the absence of the polar field. The plot shows that at sufficiently low temperatures T a low-density gas (G) phase coexists with a nematic (N) liquid. At a temperature $T = T_\mathrm{tr} \simeq 0.96$

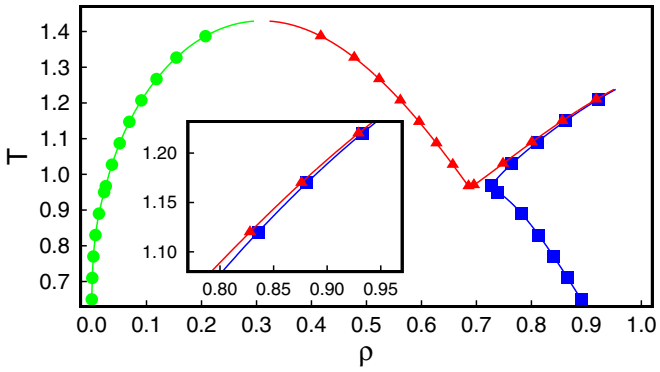

FIG. 1. The phase diagram of the liquid crystal in temperature (T)–density (ρ) representation for $\varepsilon' = 0.40$ [see Eq. (2.7b)] and $H_n = 5.0 \times 10^{-2}$ [see Eq. (2.16)]; (■) N, (▲), L, (●) G phases (see text). The inset shows an enhancement of a part of the phase diagram.

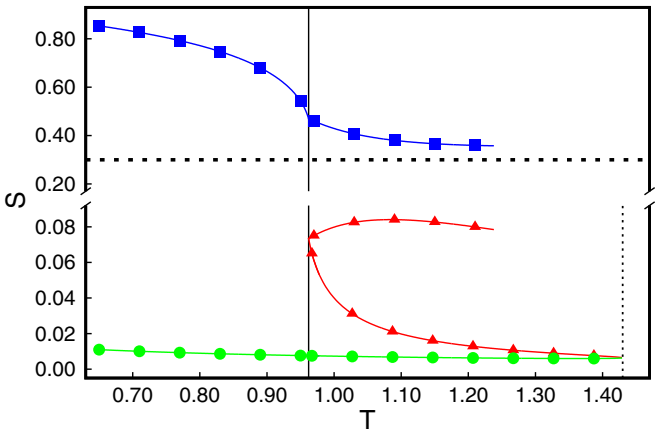

FIG. 2. Plots of the nematic order parameter S as a function of temperature T along the various phase boundaries shown in Fig. 1; (●) G, (▲) L, and (■) N phases. The vertical lines demarcate $T = T_{tr}$ (——) and $T = T_c$ (- - -), respectively. The horizontal line (· · ·) represents the threshold value $S_{LdG} = \frac{1}{3}$ obtained from the LdG theory (see text). In the curve corresponding to the L phase, the upper branch refers to phase coexistence with the N phase whereas the lower branch is computed at coexistence with G phase (see Fig. 1). Note the different scales used on the ordinate.

a triple point exists at which G and N phases coexist with an "ordinary" (i.e., nearly isotropic) liquid phase (L) (see below).

Above T_{tr}, G, and L phases coexist until the critical point is reached where both phases lose their physical meaning. The critical temperature $T_c \simeq 1.43$ is overestimated by roughly 17% as revealed by comparing T_c in Fig. 1 with $T_c \simeq 1.219$ reported by Vega *et al.* [62] for an isotropic square-well fluid (see below).

This mismatch between our version of DFT and the computer simulation data of Vega *et al.* is a consequence of our treatment of $\mathcal{F}_0^{ex}$ at the level of a first-order perturbation approach. This quantitative inadequacy of a first-order perturbative treatment of $\mathcal{F}_0^{ex}$ is quite well understood [29]. However, no attempts are made to improve the description of the G-L portion of the phase diagram because we are eventually interested in the switching between a "normal" (i.e., nonpolar) and a polar N phase.

Nevertheless, it should be noted that strategies exist to bring the near-critical region of the phase diagram into a more or less quantitative agreement with computer simulation data [63]. The critical density $\rho_c \simeq 0.299$ obtained by Vega *et al.* [62] is in much better agreement with our value $\rho_c \simeq 0.31$. This reflects the capacity of our AMMF approach to describe packing phenomena in dense L or N phases adequately.

Notice also that there is a small contribution to $\Delta\mathcal{F}^{ex}$ from u_{aniso} even though in the isotropic phase members of the set of expansion coefficients $\{\alpha_{lm}\}_{l>0}$ of α vanish altogether. However, as already explained above $\alpha_{00} = 1/\sqrt{4\pi}$ and therefore a contribution $\beta\Delta\mathcal{F}^{ex}/V = \rho^2 u_{00}/4\pi$ exists in an isotropic phase. This is a small contribution indeed because one can easily verify from Eq. (3.18) and using the results presented in Appendix C of Ref. [29] that $\Delta\mathcal{F}^{ex}/\mathcal{F}_{sw} = \frac{1}{10}\beta\varepsilon\varepsilon'^2 = 1.6 \times 10^{-2}\beta\varepsilon$.

From this result one therefore expects the phase diagram in Fig. 1 above the triple point to correspond to that of the truly *isotropic* square-well fluid (i.e., the one for which $\varphi_{anis} = 0$) to a very good approximation. Therefore, the earlier comparison with the simulation data by Vega *et al.* [62] is regarded as being physically meaningful.

Besides the phase coexistence between G and L phases above $T \gtrsim T_{tr}$ an inspection of Fig. 1 reveals a separate coexistence between L and N phases. It turns out that in this case the two-phase region is very narrow indicating that these two phases are characterized by almost the same densities at coexistence; however, the two phases can easily be distinguished on the basis of S as we shall see shortly.

As inferred from the inset in Fig. 1 we can rule out the existence of an (unphysical) critical point at which L and N phases would lose their physical meaning. This is consistent with the LdG theory of the L-N phase transition [10]. However, one has to bear in mind that this is a purely phenomenological theory with little predictive power despite its usefulness in understanding the nature of the L-N phase transition.

A somewhat peculiar feature of our treatment is a minute residual nematic order in the G and L phases. This is a consequence of the nonvanishing external potential u_n in Eq. (2.15). Comparing S for the N and G phases in the temperature range $T \lesssim T_{tr}$ one sees from the plot in Fig. 2 that S in the N phase exceeds its counterpart in the G phase by roughly a factor of 40. For $T \gtrsim T_{tr}$, S in the N phase decreases weakly with T until it almost reaches the threshold value of the nematic order parameter at the L-N phase transition $S_{LdG} = \frac{1}{3}$ obtained from the LdG theory [43]. A slightly larger threshold value of $S \simeq 0.36$ has been reported by Püschel-Schlotthauer *et al.* on the basis of finite-size scaling for a model system closely related to the present one [40]. At $T = T_c$, the branches of S for the G and L phases merge as they must because both phases lose their physical significance at the critical point.

At this point it is instructive to consider directly the odf for a state of relatively large nematic order. The plot of α in Fig. 3(a) exhibits two relatively diffuse spots in the $\tilde{\theta}$–$\tilde{\varphi}$ plane. As we explained in Sec. V, we rotated the original coordinate system so that in the new one $\hat{\boldsymbol{n}}_{rot}$ [see Eq. (5.14)] corresponds to a point on the unit sphere in the direction of $\hat{\boldsymbol{e}}_{\tilde{y}}$. This corresponds to the spot centered on $\tilde{\theta} = \tilde{\varphi} = \frac{\pi}{2}$ in

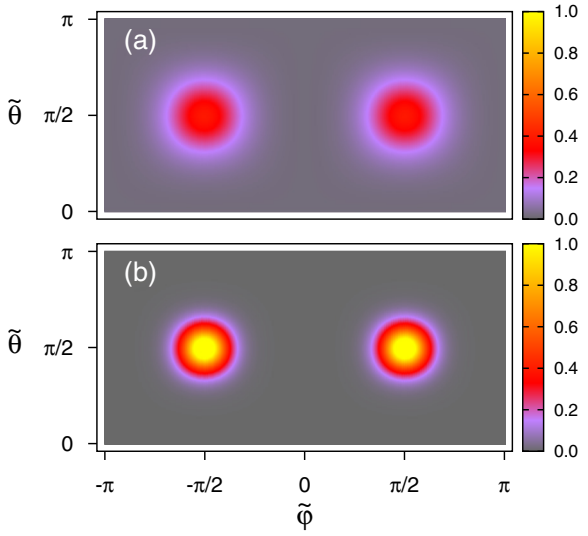

FIG. 3. The orientation distribution function $\alpha(\omega)$ in the N phase as a function of the transformed polar and azimuthal angles $\widetilde{\theta}$ and $\widetilde{\phi}$, respectively (see Sec. V). To make the plots look more symmetric, the azimuthal angle has been shifted by π so that $\widetilde{\varphi} \in [-\pi, \pi]$. The value of $\alpha(\omega)$ can be read off the attached color bars. The plots have been obtained for $H_n' = 5.0 \times 10^{-2}$ and $H_p' = 0.0$; (a) $T = 1.20$ and (b) $T = 0.75$ at phase coexistence above and below $T_{tr} \simeq 0.96$, respectively (see Fig. 1).

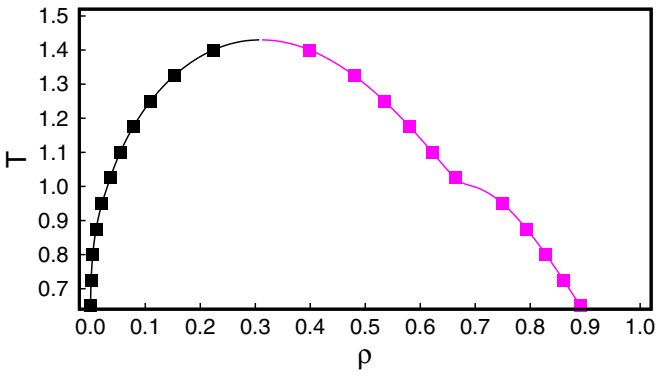

FIG. 4. As Fig. 1, but in the presence of the polar field. The phase diagram has been obtained for $H_p = 0.75$; (■) L phase, (■) G phase.

Fig. 3(a). Because one cannot distinguish between $\hat{\boldsymbol{n}}_{rot}$ and $-\hat{\boldsymbol{n}}_{rot}$ a second spot is visible in Fig. 3(a). Its center is located at the same value of $\widetilde{\theta}$ but at $\widetilde{\varphi} = -\frac{\pi}{2}$. This refers to an antipodal spot in the $-\hat{\boldsymbol{e}}_{\tilde{y}}$ direction on the surface of the unit sphere. Thus, the structure of α reflects the symmetry of the nematic phase.

The odf presented in Fig. 3(a) has been computed for $T = 1.20$. An inspection of Fig. 2 reveals that at this temperature, S in the N phase at phase coexistence is relatively low and only slightly larger than the threshold value of $S_{LdG} = \frac{1}{3}$ predicted by the LdG theory. This is reflected by the rather diffuse structure of the odf plotted in Fig. 3(a). If the temperature is lowered to $T = 0.75$ the plot of S for the N phase in Fig. 2 shows that $S \simeq 0.80$ which is more than a factor of 2 larger than S at $T = 1.20$. The structure of the odf at the lower temperature again reflects this. As the plot in Fig. 3(b) illustrates that the general symmetry of the odf remains unaltered but the spots are now much more focused and brighter. The more the spots are focused and confined to a narrow region in the $\widetilde{\theta}$-$\widetilde{\varphi}$ plane the larger is the nematic order parameter.

We also emphasize that the odf's plotted in Figs. 3(a) and 3(b) satisfy Eq. (2.13). Whereas the odf shown in Fig. 3(b) essentially vanishes outside of the two bright central spots, the corresponding plot in Fig. 3(a) is essentially nonzero everywhere in the $\widetilde{\theta}$-$\widetilde{\varphi}$ plane. This is reflected by the background in Fig. 3(a) which appears to be rather fuzzy and tinged in purple.

B. Impact of the polar field

If we now turn on the polar field $\boldsymbol{H}_p$, the width of the two-phase region happens to be remarkably insensitive as a comparison between plots in Figs. 1 and 4 indicate. However, the topology of the phase diagram changes if the polar field is turned on. Comparing the plot in Fig. 1 with the one presented in Fig. 4 one notices that for a nonvanishing polar field the coexistence between L and N phases is absent. This makes sense because with the polar field all phases are ordered to a lesser or larger extent (see also below).

However, the phase diagram in Fig. 4 exhibits a clear shoulder at about the same T and ρ at which the triple point in the plot of the corresponding phase diagram in Fig. 1 is observed. This shoulder is therefore perceived as a vestige of that triple point.

Similar effects have been observed in an earlier DFT study by Cattes *et al.* [64]. These authors studied a suspension of magnetic nanocolloids in an apolar solvent by means of classical DFT. For the orientation dependence of the interaction between the nanocolloids they adopted the classical, three-dimensional Heisenberg model.

Even though the phase diagrams for this system differ from the ones observed here, a triple point exists at which a gas phase coexists with an isotropic and a polar liquid phase. This triple point vanishes if the suspension is exposed to a sufficiently strong magnetic field. Cattes *et al.* also observed that critical lines are completely suppressed if the suspension is exposed to a magnetic field regardless of how weak this field is [64].

In general, the presence (or absence) of L-N phase coexistence can be rationalized as follows. In the absence of $\boldsymbol{H}_p$ one has two liquidlike phases of different symmetry: the N phase in which one has a well defined nematic director pointing along the z axis and the L phase that is nearly isotropic. Because of the different symmetry of both phases it is not possible to construct a continuous path in thermodynamic state space that would carry one from one phase to the other which precludes the existence of an L-N critical point [65]. This is very much akin to the situation encountered in "ordinary" liquid and solid phases. If $\boldsymbol{H}_p$ is turned on *all* phases possess a substantial amount of polar order all the way to the critical point as plots of P in Fig. 5 reveal. Thus, applying the above symmetry argument to this situation L-N phase coexistence should disappear and that is indeed what we see in Fig. 4.

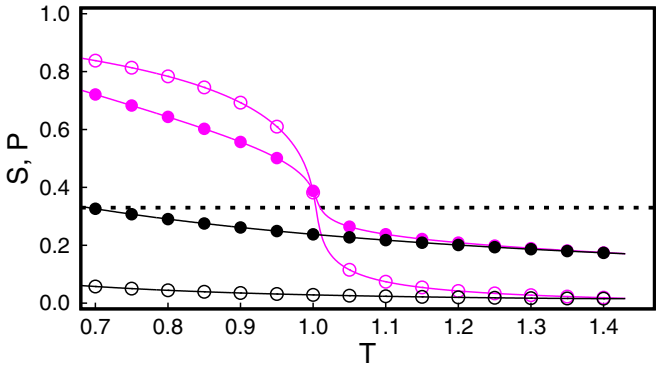

FIG. 5. Plots of the nematic order parameter S [see Eq. (5.3)] and the polarization P [see Eq. (5.8)] as functions of the temperature T; (○) S and (●) P in the N and L phases, (○) S and (●) P in the G phase. The curves have been obtained for $H_{\mathrm{p}}' = 0.75$ (see also Fig. 4). The dotted horizontal line represents $S_{\mathrm{LdG}} = \frac{1}{3}$ (see text).

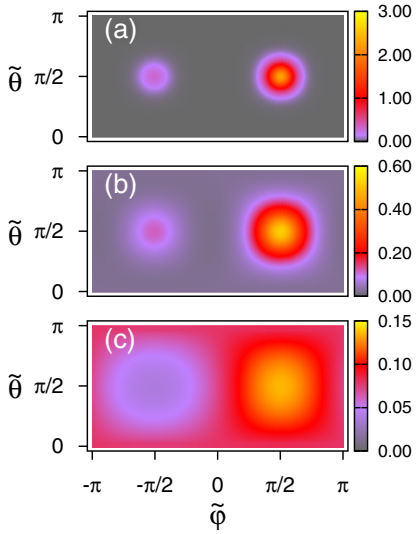

FIG. 6. As Fig. 3, but for $H_{\mathrm{p}}' = 0.75$. We emphasize the different scales used for the color bars attached to the right of each part of the figure; (a) $T = 0.75$, (b) $T = 1.00$, (c) $T = 1.20$, and the plots refer to the L phase (see Fig. 5).

We now turn to a more detailed analysis of the nematic order parameter S and the polarization P in the case of nonvanishing $\boldsymbol{H}_{\mathrm{p}}$ in Fig. 5. Plots of both quantities are now continuous functions of T because of the different topology of the corresponding phase diagram shown in Fig. 4. The plot of S for the N and L phases exhibits a sigmoidal shape with an inflection point at about the temperature $T_{\mathrm{inf}} \gtrsim T_{\mathrm{tr}} \simeq 0.96$ (see Fig. 1). Interestingly, at T_{inf}, S for the N phase agrees remarkably well with the LdG prediction [43].

At about $T \simeq T_{\mathrm{inf}}$, S in the L phase falls below the threshold value S_{LdG} obtained from the phenomenological LdG theory [43]. For $T > T_{\mathrm{inf}}$, S in the L phase decays rather quickly and approaches the low values of the nearly temperature independent curve for S in the G phase and decays monotonically. The two curves for S in the L and G phases merge at the critical point (i.e., at $T = T_{\mathrm{c}}$) at which both curves end.

The plot of P in the N and L phases reveals the same sigmoidal shape as the one for S (see Fig. 5). However, P is lower than S for $T \lesssim T_{\mathrm{inf}}$. The curves representing S and P intersect at $T \simeq T_{\mathrm{inf}}$. Beyond that intersection P exceeds S by a fair amount. P in the G phase always exceeds S and decays monotonically towards the critical point.

Whereas this observation seems to be a bit counterintuitive at first, it is relatively easy to explain. From the parity of the spherical harmonics [see Eq. (A.47) of Ref. [32]] one realizes that upon the transformation $\omega \to \omega' = -\omega = (\pi - \theta, \varphi + \pi)$, $\mathcal{Y}_{lm}(-\omega) \to -\mathcal{Y}_{lm}(\omega)$ if l is odd whereas $\mathcal{Y}_{lm}(-\omega) \to \mathcal{Y}_{lm}(\omega)$ if l is an even integer. Hence, for odd l, the transformation of the spherical harmonics is identical with that of $\hat{\boldsymbol{P}}$ [see Eqs. (5.7a)–(5.7c)], whereas for even l it is equivalent to that of $\mathbf{Q}$ [see Eq. (5.4)].

Suppose now that we have a perfectly "$\boldsymbol{P}$-like" odf that is [see Eq. (B2)]

$$\alpha_{\boldsymbol{P}}(\omega) = \sum_{\substack{2l+1 \\ m}} \alpha_{lm} \mathcal{Y}_{lm}(\omega), \quad l \in \mathbb{N}_0. \tag{6.1}$$

From the orthogonality of spherical harmonics [see Eq. (A.39) of Ref. [32]] it is then immediately clear that $\mathbf{Q} = \mathbf{0}$ because all its elements $\{\alpha_{2m}\}$ vanish identically. As a consequence, the system may have a relatively large P but $S = 0$. If α is perfectly "$\mathbf{Q}$-like" that is if

$$\alpha_{\mathbf{Q}}(\omega) = \sum_{\substack{2l \\ m}} \alpha_{lm} \mathcal{Y}_{lm}(\omega), \quad l \in \mathbb{N} \tag{6.2}$$

then $\boldsymbol{P} = \mathbf{0}$ by the same token as before. However, in general the odf will have a mixed $\boldsymbol{P}$- and $\mathbf{Q}$-like character, that is $\alpha = \zeta \alpha_{\boldsymbol{P}} + (1 - \zeta)\alpha_{\mathbf{Q}}$ where $0 \leqslant \zeta \leqslant 1$ is a mixing parameter that will depend on the strength of the fields H_{n}', H_{p}' as well as on the thermodynamic state.

On the basis of these considerations one can rationalize the plots in Fig. 5. At low T the nematic order is substantial and so is the polar order. Here the odf in the N phase should possess nearly equal amounts of $\boldsymbol{P}$- and $\mathbf{Q}$-like character. Towards $T \simeq T_{\mathrm{inf}}$ the $\mathbf{Q}$-like character of α is lost rather quickly whereas its $\boldsymbol{P}$-like character prevails all the way to the critical point.

In the G phase nematic order is rather weak indicated by low values of S regardless of T. This is because the small value of $H_{\mathrm{n}}' = 5.0 \times 10^{-2}$ causes only a minute amount of residual nematic order in the G phase which in the absence of H_{n} would be isotropic. The relatively strong polar field with $H_{\mathrm{p}}' = 0.75$ causes a fair amount of polar order in the G phase until the critical temperature has been reached. The weak monotonic decay of P is due to the enhanced thermal energy in the system as $T \to T_{\mathrm{c}}$.

These features are corroborate by the odf presented in Fig. 6. The plot of α in Fig. 6(a) exhibits two peaks as in Figs. 3(a) and 3(b) located at the same positions. The spherical symmetry of each peak of the odf already noted for $H_{\mathrm{p}}' = 0$ and their localization in the $\tilde{\theta}$-$\tilde{\varphi}$ plane is also preserved, only this time the maximum of α at $\tilde{\varphi} = -\frac{\pi}{2}$ is smaller than the one at $\tilde{\varphi} = \frac{\pi}{2}$.

The relative sharpness and this asymmetry in the peak height together indicate that the odf is of mixed $\boldsymbol{P}$ and $\mathbf{Q}$ type.

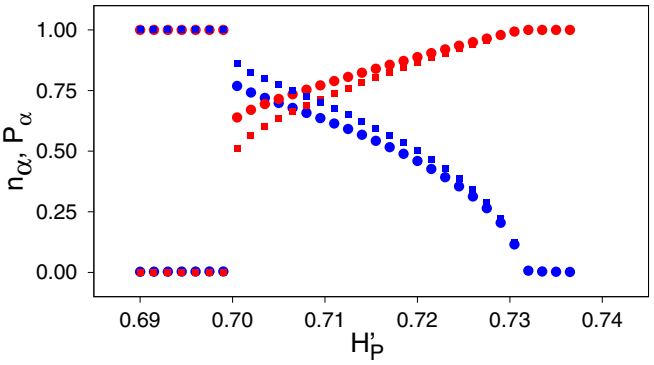

FIG. 7. Plots of components n_α of the nematic director $\hat{\boldsymbol{n}}$ and of components P_α of the unit polarization vector $\hat{\boldsymbol{P}}$ as functions of the coupling constant $H'_{\rm p}$; (■) $n_{\rm x}$, (■) $n_{\rm z}$; (●) $P_{\rm x}$, (●) $P_{\rm z}$. The curves have been obtained for $H'_{\rm n} = 1.25 \times 10^{-1}$ at a temperature $T = 0.85$.

This also suggests that part of the **Q**-type structure of the odf is submerged by the ***P***-like peak at $\widetilde{\varphi} = \frac{\pi}{2}$. According to the above line of arguments one would anticipate a relatively large value of both S and P. This is indeed what one observes from the corresponding plots of both quantities for the N phase in Fig. 5.

As T increases the plot of α in Fig. 6(b) reveals a number of interesting characteristics. First, the maxima of the odf are reduced four to five times compared with the plot in Fig. 6(a). Second, the spots of α are less localized at points in the $\widetilde{\theta}$-$\widetilde{\varphi}$ plane. This holds in particular for the **Q**-like structure in the lower half of the $\widetilde{\theta}$-$\widetilde{\varphi}$ plane (i.e., for $\widetilde{\varphi} < 0$). The more diffuse structure of $\alpha_{\mathbf{Q}}$ suggests that S decreases; the more localized structure of $\alpha_{\boldsymbol{P}}$ suggests that P remains relatively high and that is indeed what is reflected by the plots of both quantities in Fig. 5 in the higher-density phase.

Finally, at the highest T the plot in Fig. 6(c) shows that the maximum of α at $\widetilde{\theta} = \frac{\pi}{2}$ and $\widetilde{\varphi} = \frac{\pi}{2}$ is again reduced by a factor of about 4 compared with the same spot in Fig. 6(b). The **Q**-type structure of the odf is completely lost except for a hardly visible ring of slightly higher values of α; only the ***P***-like structure is still clearly visible but has become rather diffuse. This explains why at $T = 1.20$, S in the L phase is quite low whereas P still remains rather substantial as the plot in Fig. 5 indicates.

C. Switching between nonpolar and polar nematic phases

To illustrate the coupling between nonpolar and polar nematic order we plot in Fig. 7 components of the nematic director $\hat{\boldsymbol{n}}$ and of the unit polarization vector $\hat{\boldsymbol{P}}$ as functions of the coupling strength of the polar field $H'_{\rm p}$. The plots illustrate the reorientation process that takes place when the strength of the polar field increases. For $H'_{\rm p} \lesssim 0.70$ one sees that $\hat{\boldsymbol{n}}$ and $\hat{\boldsymbol{P}}$ are aligned with $\boldsymbol{H}_{\rm n}$ (i.e., the z axis) and $\boldsymbol{H}_{\rm p}$ (i.e., the x axis), respectively. Apparently, the polar field is still too weak to interfere with the orientation of $\hat{\boldsymbol{n}}$ enforced by $\boldsymbol{H}_{\rm n}$; components of $\hat{\boldsymbol{n}}$ and $\hat{\boldsymbol{P}}$ remain constant at first as $H'_{\rm n}$ increases.

At about $H'_{\rm p} \simeq 0.70$ components of $\hat{\boldsymbol{n}}$ and $\hat{\boldsymbol{P}}$ exhibit discontinuous changes. For example, $n_{\rm x}$ jumps to about 0.50 whereas $n_{\rm z}$ drops from 1.00 to about 0.87. This indicates a misalignment of $\hat{\boldsymbol{n}}$ with the z axis.

One also notices from Fig. 7 that $n_{\rm x} < P_{\rm x}$ and that $n_{\rm z} > P_{\rm z}$ at the threshold field strength of $H'_{\rm p} \simeq 0.70$. This illustrates that first upon rotation towards the x axis, $\hat{\boldsymbol{n}}$ lags behind $\hat{\boldsymbol{P}}$. Second, it shows that in any realistic treatment of the switching process, $\hat{\boldsymbol{n}}$ and $\hat{\boldsymbol{P}}$ should be treated as independent degrees of freedom as pointed out earlier by Jarkova *et al.* [15].

Rather than looking at components of $\hat{\boldsymbol{n}}$ and $\hat{\boldsymbol{P}}$ separately as in Fig. 7, it might also be instructive to look at the angle $\vartheta = \arccos(\hat{\boldsymbol{n}} \cdot \hat{\boldsymbol{P}})$ as a function of the coupling constant $H'_{\rm p}$ of the polar field $\boldsymbol{H}_{\rm p}$ (see Fig. 8). For $H_{\rm p} \lesssim 0.70$ the angle between the two vectors $\hat{\boldsymbol{n}}$ and $\hat{\boldsymbol{P}}$ turns out to be $\vartheta = 90^\circ$ and does not exhibit any dependence on $H'_{\rm p}$. Thus the rigid alignment approximation of Brochard and de Gennes [14] is invalid for coupling strengths of $H_{\rm p} \lesssim 0.70$.

At the threshold $H_{\rm p} \simeq 0.70$, ϑ drops discontinuously to about 10°. This indicates that now $\hat{\boldsymbol{n}}$ and $\hat{\boldsymbol{P}}$ are pointing in some direction in the x-z plane but that they are not collinear. The relatively small value of ϑ indicates that now the rigid anchoring assumption is satisfied to a good approximation. Further increase of $H_{\rm p}$ then causes ϑ to decrease monotonically reflecting the increasing validity of the rigid anchoring approximation. Finally, this approximation becomes exact for all values of $H_{\rm p}$ larger than the one at which $\vartheta = 0$ for the first time. Thus, in this regime $\hat{\boldsymbol{n}}$ and $\hat{\boldsymbol{P}}$ are collinear vectors as conjectured by Brochard and de Gennes [14].

Notice in particular that at $H'_{\rm p} = 0.75$, $\hat{\boldsymbol{n}}$ and $\hat{\boldsymbol{P}}$ are fully aligned with each other. Hence with respect to the phase diagram presented in Fig. 4 this means that on the high-density side we are dealing with liquid phases characterized by the same symmetry all the way to the critical point. Thus, applying the rationale of Landau and Lifshitz [65] this observation corroborates our finding that the separate L-N phase coexistence shown in Fig. 1 should disappear in the presence of (a sufficiently strong) polar field.

Even though the switching process in the x-z plane is illustrated by the plots in Fig. 7, these plots do not permit us to conclude anything about the physical nature of the phases before and after the threshold value of $H'_{\rm n} \simeq 0.70$. To unravel the quality of the phases participating in the switching process it is instructive to plot the nematic order parameter S and the polarization P as functions of the coupling constant $H'_{\rm p}$ in Fig. 9. Not unexpectedly, S is rather insensitive to $H'_{\rm p}$ regardless of the strength of the polar field. From the magnitude of S in Fig. 9 we conclude that over the whole range of $H'_{\rm p}$ considered we are dealing with a nematic phase.

However, for $H_{\rm p} \lesssim 0.70$, P attains a minute positive value which is independent of $H'_{\rm p}$. Thus, for $H_{\rm p} \lesssim 0.70$ the liquid crystal is approximately nonpolar. At $H_{\rm p} \simeq 0.70$, where all four curves in Fig. 7 exhibit a discontinuity, P in Fig. 9 changes discontinuously as well as one might have guessed. When this happens a polar nematic phase is thermodynamically stable as one infers from the magnitude of P. For $H_{\rm p} \gtrsim 0.70$, P increases monotonically until it reaches a plateau at about $H'_{\rm p} \simeq 0.73$. This plateau corresponds to the maximum polarization possible under the present thermodynamic conditions.

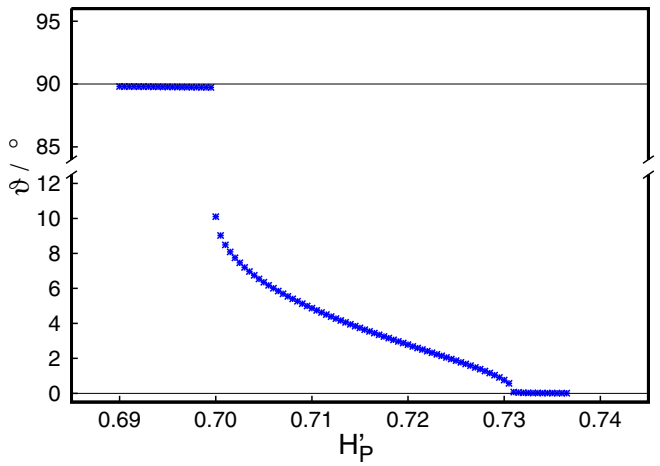

FIG. 8. Plot of the angle ϑ as a function of the coupling strength H_p' of the polar field $\boldsymbol{H}_p$. Notice also the broken ordinate.

Even though S in Fig. 9 varies only slightly with H_p' it also exhibits a discontinuous change at about $H_p' \simeq 0.70$. It then passes through a very weak maximum and exhibits a kink at H_p' at which P_x reaches its plateau and the polarization becomes saturated.

The nematic order parameter was measured in small angle neutron scattering (SANS) experiments for various concentrations of magnetic nanoplatelets in a ferromagnetic nematic liquid crystal as a function of the strength of an applied magnetic field by Mertelj *et al.* [66]. For a highly ordered phase ($S \approx 0.75$), the experimental data show a rather weak dependence on the strength of this field similar to our data plotted in Fig. 9.

The plots in Figs. 7–9 are fully corroborated by changes in the odf plotted in Fig. 10. For example, just before the discontinuous change in S and P shown in Fig. 9 at $H_p' = 0.700$ the plot in Fig. 10(a) shows that the odf has a nearly perfect **Q**-like structure. Here α has two maxima of equal height located at $\widetilde{\theta} = \frac{\pi}{2}$ and $\widetilde{\varphi} = \pm\frac{\pi}{2}$. This reflects that we are dealing with an unpolar nematic phase. This conclusion is supported by Fig. 9 which shows that $S \simeq 0.754$ and $P \simeq 0.05$ at $H_p' \lesssim\simeq 0.70$.

At a slightly larger value of $H_p' = 0.701$ the plot in Fig. 10(b) reveals that now we have an odf that has mixed **Q**- and ***P***-like character. This is reflected by the unequal height

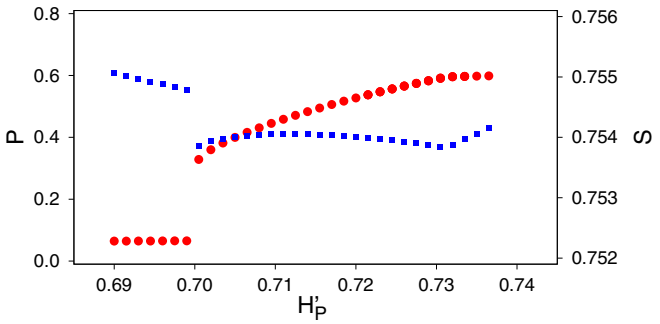

FIG. 9. As Fig. 7, but for the nematic order parameter S (■) (right ordinate) and the polarization P (●) (left ordinate) (cf. Fig. 7).

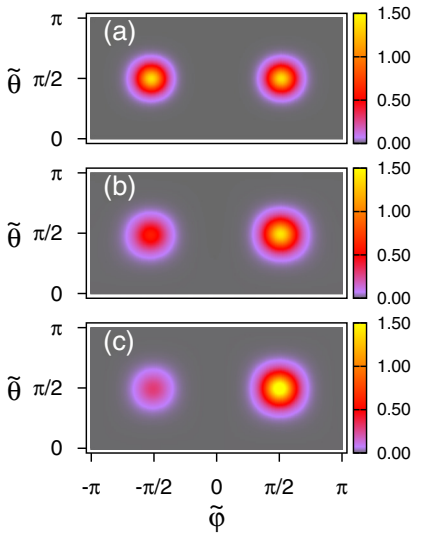

FIG. 10. As Fig. 3, but for $H_n' = 1.25 \times 10^{-1}$ and $T = 0.85$. (a) $H_p' = 0.700$, (b) $H_p' = 0.701$, (c) $H_p' = 0.731$.

of the maxima of α. Last but not least, at $H_p' = 0.731$ the odf still remains of mixed **Q**- and ***P***-like character. However, the magnitude of the maximum of α at $\widetilde{\varphi} = -\frac{\pi}{2}$ is smaller than that at $\widetilde{\varphi} = \frac{\pi}{2}$ which is now more focused and bright. This corresponds to $S \simeq 0.754$ and $P \simeq 0.60$ in Fig. 7. Hence, we conclude that a polar nematic phase is now thermodynamically stable.

VII. DISCUSSION AND CONCLUSIONS

In this paper we investigate a ferromagnetic nematic liquid crystal in an external, polar field by means of classical DFT. We believe this to be the first study of a ferromagnetic nematic liquid crystal based upon a molecular picture. The thermal behavior of our model system is governed by two elementary principles of thermodynamics stated in Eqs. (4.2) and (4.9). These lead to coupled sets of nonlinear algebraic equations [see Eqs. (4.10)–(4.12)] which we solve simultaneously and numerically.

Our key results can be summarized as follows. First, the model system is capable of forming a ferromagnetic nematic phase in the presence of a weak nematic and an orthogonal polar field. The ferromagnetic nematic phase is characterized by substantial nematic order in addition to polar order (i.e., "magnetization"). To obtain a ferromagnetic nematic phase in related experiments one is usually concerned with suspensions of magnetic nanoplatelets immersed in a nematic liquid crystal. As pointed out by Mertelj and Lisjak [16] the shape of the nanoparticles matters greatly as far as the stability is concerned. In our model system we avoid these stability issues by treating the magnetic nanoparticles *implicitly* through an additional coupling of the orientation of a liquid-crystal molecule to an external polar field. This approach has the additional advantage that we do not have to deal with a suspension. Experimentally, there are many additional problems with these suspensions, flocculation and aggregation being only two of them (see Sec. 4 of Ref. [4] for a comprehensive discussion).

Second, our simplified model system is sufficiently realistic to describe one of the key processes in ferromagnetic nematic liquid crystals, that is the capability of a reorientation of the director field in response to an external magnetic field. For example, it was demonstrated experimentally that the transmittance intensity profile varies in response to an alternating magnetic field (see Fig. 3 in Ref. [21]). This variation is a fingerprint of the periodic reorientation of the director field. The liquid crystal can thus be viewed as a switchable device.

The switching process manifests itself in our model system in various ways. First of all, we observe a threshold for the strength of the polar field beyond which the reorientation of the director field begins. The existence of such a threshold is considered to be "One of the most important discoveries in the control of [liquid crystals] by electric and magnetic fields . . . ." [23].

Another manifestation of the threshold of the strength of $\boldsymbol{H}_{\mathrm{p}}$ is the sudden change of the angle ϑ between $\hat{\boldsymbol{n}}$ and $\hat{\boldsymbol{P}}$ from 90° to about 10°. As the strength of $\boldsymbol{H}_{\mathrm{p}}$ increases beyond the threshold value, ϑ decreases continuously until it completely vanishes. This prompts us to conclude that, in line with the conjecture by by Jarkova *et al.* [15] and earlier by Burylov and Raikher [24], $\hat{\boldsymbol{n}}$ and $\hat{\boldsymbol{P}}$ should be treated as independent degrees of freedom. A second conclusion is that the so-called "rigid anchoring condition" introduced by Brochard and de Gennes [14] in their seminal work is justified to a very good approximation *beyond* the threshold value of H_{p}. However, the rigid anchoring approximation is invalid *below* the threshold. This follows from the observation that $\vartheta = 90^{\circ}$ despite the fact that in this regime the liquid crystal already possesses weak polar order.

The third key finding concerns the temperature dependence of nematic and polar order. If one raises the temperature T at a constant and sufficiently strong field $\boldsymbol{H}_{\mathrm{p}}$, the system possesses polar nematic order at lower T. Nematic order is then quickly lost as reflected by a monotonic and continuous decay of the nematic order parameter S. Whereas a similar decay is observed for the polarization P in the L phase, its polarization remains quite substantial all the way to the gas-liquid critical point.

This seemingly puzzling observation has a relatively simple explanation. For example, one realizes from the definition of P that it is related to coefficients $\{\alpha_{1m}\}$ whereas S is related to the largest eigenvalue of the alignment tensor $\mathbf{Q}$. Elements of the latter can be expressed in terms of the expansion coefficients $\{\alpha_{2m}\}$. Expansion coefficients $\{\alpha_{lm}\}$ themselves are related to spherical harmonics $\{\mathcal{Y}_{lm}\}$. For odd values of the integers l, all $\mathcal{Y}_{lm}$ exhibit point symmetry with respect to the transformation $\omega \to \omega' = -\omega$ and therefore transform like $\boldsymbol{P}$; for even l, $\mathcal{Y}_{lm}$ exhibits the same symmetry with respect to a line that is observed for $\mathbf{Q}$ upon the transformation $\omega \to \omega' = -\omega$.

One can then envision to construct a $\boldsymbol{P}$-like odf exclusively based upon coefficients $\{\alpha_{lm}\}$ for odd integers l. Likewise, one can construct a $\mathbf{Q}$-like odf based upon expansion coefficients for which l is an even integer. Because the spherical harmonics form a complete orthonormal set of basis functions, a $\boldsymbol{P}$-like odf would give nonzero values only for $\{\alpha_{1m}\}$ and vanishing coefficients $\{\alpha_{2m}\}$. In this case P would be nonzero whereas S would vanish. By the same token we can argue that a $\mathbf{Q}$-like odf would only give $P = 0$. Most odf's are composed of $\boldsymbol{P}$- and $\mathbf{Q}$-like portions and will therefore give rise to nonzero values of S and P simultaneously.

We demonstrate that in a properly rotated frame of reference the structures of $\boldsymbol{P}$- and $\mathbf{Q}$-like odf's are particularly simple. In a color-coded representation a $\mathbf{Q}$-like odf consists of two spots on the unit sphere where one is antipodal to the other. For a $\boldsymbol{P}$-like odf one of the two spots is missing owing to the (di)polar nature of the liquid crystal.

It should also be noted that regardless of the specific situation under study, the color-coded odf always exhibts two spots in the $\widetilde{\theta}$-$\widetilde{\varphi}$ plane. These spots are always radially symmetric, that is symmetric with respect to an axis through their centers and normal to the $\widetilde{\theta}$-$\widetilde{\varphi}$ plane. Therefore, the system always has uniaxial symmetry regardless of the thermodynamic conditions and the relative strengths of $\boldsymbol{H}_{\mathrm{n}}$ and $\boldsymbol{H}_{\mathrm{p}}$. The radial symmetry of the spots of the odf is the reason for why the biaxiality order parameter η is always zero.

It has recently been shown by Skutnik *et al.* [47] that a substantial biaxiality requires an odf with more than just one symmetry axis. Looking again at color-coded odf's in Fig. 7 of Ref. [47] one realizes that for phases of biaxial symmetry the odf appears to be elliptically deformed in the θ-φ' plane (which is different from the $\widetilde{\theta}$-$\widetilde{\varphi}$ plane used here). Thus, the odf has a semimajor and a semiminor axis as its symmetry elements and therefore $\eta \neq 0$ has been observed in the Monte Carlo simulations by Skutnik *et al.*

Unfortunately, we find it rather difficult to make more direct contact with experiments beyond the points discussed above. In this respect we fully agree with Garbovskiy and Glushenko [4] who state that ". . .experimental data and theoretical predictions are not easy to compare." Nevertheless, there are possible interfaces between this work and experiments that one may perhaps want to carry out in the future.

For example, one of the key ingredients of the present theory is the AMMF approximation represented by Eq. (3.8). It involves at its core the radial pair correlation function g_0 in an isotropic phase and a suitable choice for the anisotropic interaction potential u_1. The former can be obtained for molecular liquids by measuring the static structure factor in neutron scattering experiments (see Fig. 5 of Ref. [67]). Neutron scattering has also been used by Mertelj *et al.* [66] to investigate the structure of ferromagnetic nematic liquid crystals.

Using information about a molecule's electronic structure (i.e., such as multipole moments, polarizabilities, etc.; see Chap. 2 of Ref. [32]) one could devise an approximate form for u_1. With this experimental information one could then obtain an ansatz for g in Eq. (3.8) and with this all relevant information of an experimental system such as the phase diagram, details of the switching process, or the odf.

The latter can also be measured independently in electron paramagnetic resonance spectroscopy [68]. With this experimental information and with a suitable transformation through Eqs. (5.10)–(5.14) one could determine the expansion coefficients $\{\alpha_{1m}\}$ and $\{\alpha_{2m}\}$ from Eq. (4.5). This gives one access to $\boldsymbol{P}$ through Eqs. (5.7a)–(5.7c) and to $\mathbf{Q}$ from Eq. (5.4). The nematic order parameter can then be computed from Eq. (5.5c) where it needs to be stressed that all these equations

are exact. With the nematic order parameter one can solve Eq. (5.2) to obtain the nematic director $\hat{\boldsymbol{n}}$. Thus, one could investigate magneto-optic properties of the material under investigation following the analysis just outlined [19–21].

In addition, the direct measurement of the odf and its comparison with the one obtained through the protocol based upon the AMMF approximation for the orientation dependent pair correlation function one could assess quantitatively the robustness of the DFT proposed in this work.

ACKNOWLEDGMENT

One of us (M.S.) is indebted to Professor G. Jackson (Imperial College London) for fruitful discussions during the initial phase of this project.

APPENDIX A: ORIENTATION DEPENDENCE OF THE HESS-SU MODEL POTENTIAL

In this Appendix we demonstrate that the orientation dependence of u_{aniso} in Eq. (2.7b) is the same as in the model proposed by Hess and Su [31] for the special case in which only their coupling constant ϵ_1 is nonzero.

Let us define a real, symmetric, traceless, second-rank tensor [cf. Eq. (2.12)]

$$\mathbf{U}^{(i)} = \hat{\boldsymbol{u}}_i\hat{\boldsymbol{u}}_i - \tfrac{1}{3}1, \quad i = 1, 2, \tag{A1}$$

where $\mathbf{1}$ is the unit tensor and components of $\hat{\boldsymbol{u}}_i$ are defined analogously to the expressions given in Eqs. (2.14a)–(2.14c). Using Eq. (B.11) of Ref. [32] we have

$$\mathbf{U}^{(1)} : \mathbf{U}^{(2)} = U^{(1)}_{\alpha\beta}U^{(2)}_{\beta\alpha}, \tag{A2}$$

where we use the Einstein repeated index summation convention. Equations (A1) and (A2) are equivalent to Eqs. (5) and (7), respectively and to the first term on the right-hand side of Eq. (9) in the paper by Hess and Su [31]. Equation (A2) is sometimes referred to as the Frobenius inner product [69].

From Eqs. (A1) and (A2) it is easy to verify that we can rewrite the latter as

$$\begin{aligned} U^{(1)}_{\alpha\beta}U^{(2)}_{\beta\alpha} &= (\hat{\boldsymbol{u}}_1\hat{\boldsymbol{u}}_1)_{\alpha\beta}(\hat{\boldsymbol{u}}_2\hat{\boldsymbol{u}}_2)_{\beta\alpha} \\ &\quad -\tfrac{1}{3}[(\hat{\boldsymbol{u}}_1\hat{\boldsymbol{u}}_1)_{\alpha\alpha} + (\hat{\boldsymbol{u}}_2\hat{\boldsymbol{u}}_2)_{\alpha\alpha}] + \tfrac{1}{3} \\ &= (\hat{\boldsymbol{u}}_1\hat{\boldsymbol{u}}_1)_{\alpha\beta}(\hat{\boldsymbol{u}}_2\hat{\boldsymbol{u}}_2)_{\beta\alpha} - \tfrac{1}{3}, \end{aligned} \tag{A3}$$

where we have used Eqs. (B.19) of Ref. [32], the identity $\mathbf{1} : \mathbf{1} = 3$, and $(\hat{\boldsymbol{u}}_1\hat{\boldsymbol{u}}_1)_{\alpha\alpha} = (\hat{\boldsymbol{u}}_2\hat{\boldsymbol{u}}_2)_{\alpha\alpha} = 1$. We now use the identity [cf. Eq. (B.16) of Ref. [32]]

$$\hat{\boldsymbol{u}}_1\hat{\boldsymbol{u}}_1 : \hat{\boldsymbol{u}}_2\hat{\boldsymbol{u}}_2 = (\hat{\boldsymbol{u}}_1 \cdot \hat{\boldsymbol{u}}_2)^2, \tag{A4}$$

which is easy to verify. The identity then permits us to rewrite Eq. (A2) as

$$\mathbf{U}^{(1)} : \mathbf{U}^{(2)} = (\hat{\boldsymbol{u}}_1 \cdot \hat{\boldsymbol{u}}_2)^2 - \tfrac{1}{3} = \tfrac{2}{3}P_2(x), \tag{A5}$$

which is equivalent to the orientation dependence of u_{aniso} in our model [see Eq. (2.7b)] except for trivial numerical factors.

APPENDIX B: ANALYTICAL INTEGRATION OVER ORIENTATIONS

In this Appendix we present details of the integrations over orientations in Eq. (3.9). Consider the integral

$$\mathcal{I} \equiv \iiint d\omega_1\, d\omega_2\, d\omega\, \alpha(\omega_1)\alpha(\omega_2)\Phi_{l_1l_2l}(\omega_1, \omega_2, \omega). \tag{B1}$$

Because the external potential u_{ext} in Eq. (2.17) depends on the angles φ and θ, the odf will as well. Therefore, it is advantageous to expand the odf in the basis of spherical harmonics according to

$$\alpha(\omega) = \sum_{lm} \alpha_{lm}\mathcal{Y}_{lm}(\omega), \tag{B2}$$

where elements of the set $\{\alpha_{lm}\}$ are (complex) expansion coefficients. Thus, we can rewrite Eq. (B1) as

$$\begin{aligned} \mathcal{I} = \sum_{\substack{l_1l_2l \\ m_1m_2m}} C(l_1l_2l; m_1m_2m) \int d\omega\, \mathcal{Y}^*_{lm}(\omega) \\ \times \sum_{L_1M_1} \alpha_{L_1M_1} \int d\omega_1\, \mathcal{Y}_{l_1m_1}(\omega_1)\mathcal{Y}_{L_1M_1}(\omega_1) \\ \times \sum_{L_2M_2} \alpha_{L_2M_2} \int d\omega_1\, \mathcal{Y}_{l_2m_2}(\omega_2)\mathcal{Y}_{L_2M_2}(\omega_2), \end{aligned} \tag{B3}$$

where Eq. (2.4) has also been employed.

The tenfold summation in this expression can be reduced quite considerably by utilizing properties of the spherical harmonics. For example, one realizes that $\mathcal{I}$ vanishes unless $l = m = 0$ [see Eq. (A.38) of Ref. [32]]. The two selection rules for nonzero Clebsch-Gordan coefficients (see Sec. II) then imply that $l_1 = l_2$ and that $m_1 = -m_2$. Consequently the sixfold summation over l_1, l_2, l, m_1, m_2, and m collapses to a twofold one and Eq. (B3) can be simplified to

$$\begin{aligned} \mathcal{I} = \sqrt{4\pi} \sum_{lm} C(ll0; m\underline{m}0) \\ \times \sum_{L_1M_1} \alpha_{L_1M_1} \int d\omega_1\, \mathcal{Y}_{lm}(\omega_1)\mathcal{Y}_{L_1M_1}(\omega_1) \\ \times \sum_{L_2M_2} \alpha_{L_2M_2} \int d\omega_1\, \mathcal{Y}_{l\underline{m}}(\omega_2)\mathcal{Y}_{L_2M_2}(\omega_2). \end{aligned} \tag{B4}$$

Because the spherical harmonics form a complete set of orthonormal basis functions, the remaining two integrations vanish (see Eq. (A.39) of Ref. [32]) unless $l = L_1 = L_2$, $\underline{m} = M_1$, and $m = M_2$. This permits us to rewrite Eq. (B4) compactly as

$$\mathcal{I} = \sqrt{4\pi} \sum_{lm} \frac{(-1)^{l+m}}{\sqrt{2l+1}} \alpha_{lm}\alpha_{l\underline{m}}, \tag{B5}$$

where Eqs. (A.3) und (A.150) of Ref. [32] have also been used.

APPENDIX C: ANALYSIS OF Q IN AN IDEALIZED SYSTEM

In this Appendix we will demonstrate the validity of the expressions presented in Eqs. (5.5a)–(5.6). Focusing on the

x-z plane we choose an idealized odf expressed as [see Eq. (A.32) of Ref. [32]]

$$\alpha(\omega) = \tfrac{1}{2}[\delta(\omega-\omega') + \delta(\omega+\omega')] = \tfrac{1}{2}[\delta(x-x')\delta(\varphi) + \delta(x+x')\delta(\varphi+\pi)], \quad \text{(C1)}$$

where we use the shorthand notation $x = \cos\theta$ and $x' = \cos\theta'$. This idealized odf represents two infinitely sharp peaks located on opposite sides of the unit sphere. The underlying assumption is that the liquid crystal is perfectly ordered along some direction in the x-z plane. This form of the odf also reflects the indistinguishability of $\hat{\boldsymbol{n}}$ and $-\hat{\boldsymbol{n}}$ in the nematic phase [cf., Figs. 3(a) and 3(b)]. Because of this symmetry it turns out that each of the two products of δ functions generates the same result. Thus, we can replace Eq. (C1) by the simpler expression

$$\alpha(\omega) = \delta(x-x')\delta(\varphi). \quad \text{(C2)}$$

From Eq. (4.5) we therefore obtain

$$\alpha_{20} = \sqrt{\frac{5}{4\pi}}\int_{-1}^{1} dx\,\frac{1}{2}(3x^2-1)\delta(x-x')\int_0^{2\pi} d\varphi\,\delta(\varphi) = \sqrt{\frac{5}{4\pi}}\int_{-1}^{1} dx\,\frac{1}{2}(3x^2-1)\delta(x-x') = \sqrt{\frac{5}{4\pi}}\frac{1}{2}(3x'^2-1), \quad \text{(C3)}$$

where we utilized the well-known properties of the Dirac δ function. By essentially the same algebraic manipulations we obtain

$$\mathrm{Re}\,\alpha_{21} = \sqrt{\frac{5}{4\pi}}\sqrt{\frac{3}{2}}x'\sqrt{1-x'^2}, \quad \text{(C4a)}$$

$$\mathrm{Re}\,\alpha_{22} = \sqrt{\frac{5}{4\pi}}\sqrt{\frac{3}{8}}(1-x'^2). \quad \text{(C4b)}$$

A couple of comments apply at this point. First, the integral over $d\varphi$ on the first line of Eq. (C3) is unity on account of the definition of the Dirac δ function. Second, replacing the product of the two δ functions by the other term in Eq. (C1) would not change anything because x enters the integrand in Eq. (C3) quadratically.

A more subtle point arises seemingly because for α_{21} and α_{22} the integrand contains a factor of $e^{im\varphi}$ where $m = 1, 2$. Thus, the integral involving

$$\int_0^{2\pi} d\varphi\,[\cos(m\varphi) + i\sin(m\varphi)]\delta(\varphi) = 1 \quad \text{(C5)}$$

whereas

$$\int_0^{2\pi} d\varphi\,[\cos(m\varphi) + i\sin(m\varphi)]\delta(\varphi+\pi) = (-1)^m. \quad \text{(C6)}$$

The integrands leading to the expressions given in Eqs. (C4a) and (C4b) are of the general form,

$$\int_{-1}^{1} dx\,f(x)[\delta(x-x') + (-1)^m\delta(x+x')],$$

where $f(x) = -f(-x)$ in the case of $\mathrm{Re}\,\alpha_{21}$ whereas $f(x) = f(-x)$ for $\mathrm{Re}\,\alpha_{22}$. Thus, even in case of $\mathrm{Re}\,\alpha_{21}$ using the full odf as introduced in Eq. (C1) would only generate two times the expression given in Eq. (C4a).

With the expressions derived in Eqs. (C3) and (C4b) it therefore follows from Eq. (5.5a) that $\lambda_- = -\frac{1}{2}$; one also finds from Eqs. (5.5b) and (5.5c) that $\lambda_0 = \frac{1}{4} - \frac{\Delta}{2}$ and $\lambda_+ = \frac{1}{4} + \frac{\Delta}{2}$, respectively. Using Eqs. (C3)–(C4b) we can also compute

$$\Delta = \frac{3}{2}\sqrt{\frac{1}{4}(2-4x'^2)^2 + 4x'^2(1-x'^2)} = \frac{3}{2} \quad \text{(C7)}$$

from Eq. (5.6).

Consequently, for the idealized odf introduced in Eq. (C1) we obtain $\lambda_0 = \lambda_- = -\frac{1}{2}$ and $\lambda_+ = 1$. From Eq. (5.3) this gives $S = 1$. Perhaps not surprisingly, the eigenvectors associated with λ_-, λ_0, and λ_+ are given by $\hat{\boldsymbol{n}}_-^{\mathrm{T}} = (0, 1, 0)$, $\hat{\boldsymbol{n}}_0^{\mathrm{T}} = (\cos\theta, 0, \sin\theta)$, and $\hat{\boldsymbol{n}}_+^{\mathrm{T}} = (-\sin\theta, 0, \cos\theta)$.

[1] M. Camacho-Lopez, H. Finkelmann, P. Palffy-Muhoray, and M. Shelley, Nat. Mater. **3**, 307 (2004).
[2] A. B. G. M. Leferink op Reinink, E. van den Pol, A. V. Petukhov, G. J. Vroege, and H. N. W. Lekkerkerker, Eur. Phys. J.: Spec. Top. **222**, 3053 (2013).
[3] H. Kikuchi, M. Yokota, Y. Hisakado, H. Yang, and T. Kajiyama, Nat. Mater. **1**, 64 (2002).
[4] Y. Garbovskiy and A. Glushchenko, Nanomaterials **7**, 361 (2017).
[5] J.-H. Kim, M. Yoneya, and H. Yokoyama, Nature (London) **420**, 159 (2002).
[6] P. Malik and K. K. Raina, Opt. Mater. **27**, 613 (2004).
[7] W. Hu, H. Zhao, L. Song, Z. Yang, H. Cao, Z. Cheng, Q. Liu, and H. Yang, Adv. Mater. **22**, 468 (2010).
[8] E. van den Pol, A. V. Petukhov, D. M. E. Thies-Weesie, D. V. Byelov, and G. J. Vroege, Phys. Rev. Lett. **103**, 258301 (2009).
[9] T. Ostapenko, D. B. Wiant, S. N. Sprunt, A. Jákli, and J. T. Gleeson, Phys. Rev. Lett. **101**, 247801 (2008).
[10] P. G. de Gennes and J. Prost, *The Physics of Liquid Crystals*, 2nd ed. (Oxford Science Publications, Oxford, 1995).
[11] W. Maier and A. Saupe, Z. Naturforsch. A **15**, 287 (1960).
[12] M. Born, Sitz. Kön. Preuss. Akad. Wiss. **30**, 614 (1916).
[13] M. Born, Ann. Phys. **360**, 177 (1918).
[14] F. Brochard and P. G. de Gennes, J. Phys. **31**, 691 (1970).
[15] E. Jarkova, H. Pleiner, H.-W. Müller, A. Fink, and H. R. Brand, Eur. Phys. J. E **5**, 583 (2001).
[16] A. Mertelj and D. Lisjak, Liq. Cryst. Rev. **5**, 1 (2017).
[17] A. Mertelj, D. Lisjak, M. Drofenik, and M. Čopič, Nature (London) **504**, 237 (2013).
[18] M. Shuai, A. Klittnick, Y. Shen, G. P. Smith, M. R. Tuchband, C. Zhu, R. G. Petschek, A. Mertelj, D. Lisjak, M. Čopič, J. E. MacLennan, M. A. Glaser, and N. A. Clark, Nat. Commun. **7**, 10394 (2016).
[19] T. Potisk, D. Svenšek, H. R. Brand, H. Pleiner, D. Lisjak, N. Osterman, and A. Mertelj, Phys. Rev. Lett. **119**, 097802 (2017).

[20] T. Potisk, A. Mertelj, N. Sebastián, N. Osterman, D. Lisjak, H. R. Brand, H. Pleiner, and D. Svenšek, Phys. Rev. E **97**, 012701 (2018).

[21] M. Wang, L. He, S. Zorba, and Y. Yin, Nano Lett. **14**, 3966 (2014).

[22] S. Gao, M. Fleisch, R. A. Rupp, L. Cmok, P. Medle-Rupnik, A. Mertelj, D. Lisjak, X. Zhang, and I. Drevenšek-Olenik, Opt. Express **27**, 8900 (2019).

[23] V. Gdovinová, N. Tomašovičová, N. Éber, P. Salamon, T. Tóth-Katona, V. Závišová, J. Kováč, J. Jadżyn, and P. Kopčanský, Phase Transit. **90**, 780 (2017).

[24] S. V. Burylov and Y. L. Raikher, Mol. Cryst. Liq. Cryst. **258**, 107 (1995).

[25] S. V. Burylov and Y. L. Raikher, Mol. Cryst. Liq. Cryst. **258**, 123 (1995).

[26] H. Pleiner, E. Jarkova, H.-W. Müller, and H. R. Brand, Magnetohydrodynamics **37**, 146 (2001).

[27] V. I. Zadorozhnii, A. Vasilev, V. Y. Reshetnyak, K. S. Thomas, and T. J. Sluckin, Europhys. Lett. **73**, 408 (2005).

[28] V. I. Zadorozhnii, T. J. Sluckin, V. Y. Reshetnyak, and K. S. Thomas, SIAM J. Appl. Math. **68**, 1688 (2008).

[29] M. Schoen, A. J. Haslam, and G. Jackson, Langmuir **33**, 11345 (2017).

[30] M. Greschek and M. Schoen, Phys. Rev. E **83**, 011704 (2011).

[31] S. Hess and B. Su, Z. Naturforsch. A **54**, 559 (1999).

[32] C. G. Gray and K. E. Gubbins, *Theory of Molecular Fluids* (Clarendon, Oxford, 1984), Vol. 1.

[33] F. Franco-Melgar, Ph.D. thesis, Imperial College London, 2006.

[34] M. Franco-Melgar, A. J. Haslam, and G. Jackson, Mol. Phys. **107**, 2329 (2009).

[35] H. Steuer, S. Hess, and M. Schoen, Physica A **328**, 322 (2003).

[36] H. Steuer, S. Hess, and M. Schoen, Phys. Rev. E **69**, 031708 (2004).

[37] M. Greschek, K. E. Gubbins, and M. Schoen, J. Chem. Phys. **137**, 144703 (2012).

[38] T. Stieger, M. Schoen, and M. G. Mazza, J. Chem. Phys. **140**, 054905 (2014).

[39] S. M. Wandrei, R. Roth, and M. Schoen, J. Chem. Phys. **149**, 054704 (2018).

[40] S. Püschel-Schlotthauer, T. Stieger, M. Melle, M. G. Mazza, and M. Schoen, Soft Matter **12**, 469 (2016).

[41] P. Poulin and D. A. Weitz, Phys. Rev. E **57**, 626 (1998).

[42] I. I. Smalyukh, O. D. Lavrentovich, A. N. Kuzmin, A. V. Kachynski, and P. P. N. Prasad, Phys. Rev. Lett. **95**, 157801 (2005).

[43] S. Püschel-Schlotthauer, Ph.D. thesis, Technische Universität Berlin, 2017.

[44] S. Püschel-Schlotthauer, V. M. Turrión, C. K. Hall, M. G. Mazza, and M. Schoen, Langmuir **33**, 2222 (2017).

[45] K. P. Zuhail, P. Sathyanarayana, D. Seč, S. Čopar, M. Škarabot, I. Muševič, and S. Dhara, Phys. Rev. E **91**, 030501(R) (2015).

[46] K. P. Zuhail and S. Dhara, Appl. Phys. Lett. **106**, 211901 (2015).

[47] R. A. Skutnik, L. Lehmann, S. Püschel-Schlotthauer, G. Jackson, and M. Schoen, Mol. Phys. (2019), doi: 10.1080/00268976.2019.1581292.

[48] M. Greschek, M. Melle, and M. Schoen, Soft Matter **6**, 1898 (2010).

[49] A. A. Sonin, *The Surface Physics of Liquid Crystals* (Gordan and Breach, Amsterdam, 1995).

[50] K. E. Gubbins and C. G. Gray, Mol. Phys. **23**, 187 (1972).

[51] N. F. Carnahan and K. E. Starling, J. Chem. Phys. **51**, 635 (1969).

[52] J.-P. Hansen and I. R. McDonald, *Theory of Simple Liquids*, 4th ed. (Academic, New York, 2013).

[53] J. A. Barker and D. Henderson, J. Chem. Phys. **47**, 2856 (1967).

[54] R. W. Zwanzig, J. Chem. Phys. **22**, 1420 (1954).

[55] R. W. Zwanzig, J. Chem. Phys. **22**, 2099 (1954).

[56] A. Gil-Villegas, A. Galindo, P. J. Whitehead, S. J. Mills, G. Jackson, and A. N. Burgess, J. Chem. Phys. **106**, 4168 (1997).

[57] Note that this implicitly assumes that solutions of Eqs. (4.2) do not correspond to maxima instead of minima of Ω; strictly speaking, this would need to be verified separately .

[58] W. H. Press, S. A. Teukolsky, W. T. Vetterling, and B. P. Flannery, in *Numerical Recipes: The Art of Scientific Computing*, 3rd ed. (Cambridge University Press, Cambridge, UK, 2007), Chap. 11.1.

[59] R. Eppenga and D. Frenkel, Mol. Phys. **52**, 1303 (1984).

[60] M. Gramzow and S. H. L. Klapp, Phys. Rev. E **75**, 011605 (2007).

[61] M. P. Allen and D. J. Tildesley, *Computer Simulation of Liquids*, 2nd ed. (Oxford University Press, Oxford, 2017).

[62] L. Vega, E. de Miguel, L. F. Rull, G. Jackson, and I. A. McLure, J. Chem. Phys. **96**, 2296 (1992).

[63] T. Lafitte, A. Apostolakou, C. Avendaño, A. Galindo, C. S. Adjiman, E. A. Müller, and G. Jackson, J. Chem. Phys. **139**, 154504 (2013).

[64] S. M. Cattes, S. H. L. Klapp, and M. Schoen, Phys. Rev. E **91**, 052127 (2015).

[65] L. D. Landau and E. M. Lifshitz, in *Course of Theoretical Physics* (Elsevier, Amsterdam, 2013), Vol. 5, Chap. 8, pp. 257–260.

[66] A. Mertelj, B. Lampret, D. Lisjak, J. Klepp, J. Kohlbrecher, and M. Copic, Soft Matter **15**, 5412 (2019).

[67] D. Morineau, R. Guégan, Y. Xia, and C. Alba-Simionesco, J. Chem. Phys. **121**, 1466 (2004).

[68] T. S. Yankova, A. Y. Bobrovsky, and A. K. Vorobiev, J. Phys. Chem. B **116**, 6010 (2012).

[69] R. A. Horn and C. R. Johnson, *Matrix Analysis*, 2nd ed. (Cambridge University Press, Cambridge, UK, 1990).